

A comparison between microscopic methods for finite temperature Bose gases

S.P. Cockburn^{1,*}, A. Negretti^{2,3}, N.P. Proukakis¹, and C. Henkel⁴

1. School of Mathematics and Statistics, University of Newcastle upon Tyne, Newcastle upon Tyne, NE1 7RU, United Kingdom

2. Lundbeck Foundation Theoretical Center for Quantum System Research,

Department of Physics and Astronomy, Aarhus University, 8000 Aarhus C, Denmark

3. Institut für Quanteninformationsverarbeitung, Universität Ulm, Albert- Einstein-Allee 11, 89069 Ulm, Germany

4. Institut für Physik und Astronomie, Universität Potsdam,

Karl-Liebknecht-Str. 24-25, 14476 Potsdam, Germany

(Dated: Tues 7 Dec 2010)

We analyze the equilibrium properties of a weakly interacting, trapped quasi-one-dimensional Bose gas at finite temperatures and compare different theoretical approaches. We focus in particular on two stochastic theories: a number-conserving Bogoliubov (ncB) approach and a stochastic Gross-Pitaevskii equation (sGPe) that have been extensively used in numerical simulations. Equilibrium properties like density profiles, correlation functions, and the condensate statistics are compared to predictions based upon a number of alternative theories. We find that due to thermal phase fluctuations, and the corresponding condensate depletion, the ncB approach loses its validity at relatively low temperatures. This can be attributed to the change in the Bogoliubov spectrum, as the condensate gets thermally depleted, and to large fluctuations beyond perturbation theory. Although the two stochastic theories are built on different thermodynamic ensembles (ncB: canonical, sGPe: grand-canonical), they yield the correct condensate statistics in a large BEC (strong enough particle interactions). For smaller systems, the sGPe results are prone to anomalously large number fluctuations, well-known for the grand-canonical, ideal Bose gas. Based on the comparison of the above theories to the modified Popov approach, we propose a simple procedure for approximately extracting the Penrose-Onsager condensate from first- and second-order correlation functions that is computationally convenient. This also clarifies the link between condensate and quasi-condensate in the Popov theory of low-dimensional systems.

PACS numbers: 03.75.Hh; 67.85.-d; 67.85.Bc; 05.10.Gg; 42.50.-p

Contents		III. Equilibrium properties	12
I. Introduction	2	A. Density profile	12
II. Simulation techniques under consideration	4	B. Condensate and thermal excitations	15
A. Truncated Wigner	4	1. Density profiles and depletion	15
B. Number conserving Bogoliubov initial state	5	2. Condensate shape	16
1. Condensate mode	5	C. Correlation functions	17
2. Elementary excitations	5	1. First-order coherence: phase fluctuations.	18
3. Condensate number	6	2. Second-order coherence: density fluctuations	19
4. Validity range	6	3. Squeezing and anomalous average	20
C. Stochastic Gross-Pitaevskii equation	7	D. Condensate statistics and fragmentation	21
1. System plus bath split	7	1. Counting statistics	21
2. Stochastic equation of motion	7	2. Discussion	23
3. Damping and noise	8	3. Fragmentation	24
4. Validity range	8	IV. Condensation vs. quasi-condensation	24
5. State preparation	8	A. Identifying the quasi-condensate	25
D. Linking the theories	9	B. Identifying the Penrose-Onsager condensate density	25
E. Modified Popov theory	10	C. Application: (quasi) condensate fraction	26
1. Motivation	10	V. Slow thermalization of the initial state	27
2. Quasi-condensate density	10	VI. Conclusions	29
F. Parameter choice for comparison	11	A. Sampling the number-conserving Bogoliubov state	30

*E-mail: s.p.cockburn@ncl.ac.uk

B. Canonical counting statistics of a Bose gas	31
References	33

I. INTRODUCTION

Following the first observation of Bose-Einstein condensation of dilute gases, experimental and theoretical efforts were mainly focused on the fundamental properties of such degenerate quantum gases, including spatial and momentum distributions, and collective excitations [1, 2]. Mean field theory was initially found to be impressively successful in most cases. Indeed, at temperatures well below the phase transition, nearly all atoms occupy one wave function that satisfies a nonlinear Schrödinger equation, the celebrated Gross-Pitaevskii equation (GPe). The nonlinear term describes the mean field potential experienced by the atoms due to two-body interactions. In the language of quantum field theory, the GPe yields a zeroth-order approximation to the full matter-wave field where both the non-condensed component of the gas and quantum fluctuations are neglected.

The Bogoliubov theory provides an improved analysis of this system by including small fluctuations around the condensate wave function. Its predictions include, e.g., the spectrum of collective excitations, the quantum depletion of the condensate, and correlation functions at both zero and nonzero temperature. We focus in this paper on a one-dimensional trapped gas as a model for a weakly interacting quasi-one-dimensional system confined tightly in the radial direction. In such a system, the contribution of low-energy modes is significant. From Bogoliubov theory, these modes mainly affect the phase of the matter-wave field, the density fluctuations being relatively weak. As a consequence, there is no Bose condensate in the homogeneous limit. Still, a so-called quasi-condensate can be identified where long-range coherence manifests itself in the suppression of density fluctuations, while the phase is correlated only over distances smaller than the system size [3–8]. The situation is similar to a “fragmented” condensate where several low-energy modes appear with comparable weight [9].

The (quasi-)condensate and atoms in excited states (“thermal cloud”) are often treated as two subsystems that are coupled to each other by scattering processes that exchange particles and energy. Approaches based on such a splitting between condensate and thermal dynamics lead to a generalized GPe for the condensate dynamics that differs from its $T = 0$ counterpart through the inclusion of the thermal cloud mean field (Hartree-Fock potential). In addition, a source term may describe the scattering of particles between the condensate and thermal cloud [10, 11]. The thermal cloud itself is described by a quantum Boltzmann

equation [12–14] self-consistently coupled to the condensate [15–19]. In its kinetic formulation, the resulting self-consistent, coupled Gross-Pitaevskii-Boltzmann approach, which extends earlier work by Kirkpatrick and Dorfman [20], and Eckern [21], is often referred to as the “ZNG” scheme within the context of trapped atomic gases [15, 22]. This method reproduces the two-fluid hydrodynamics in the collisional, hydrodynamic regime [23, 24], and has been tested successfully against experiment for collective modes [25–27] and macroscopic excitations [28, 29]. Since the ZNG approach is numerically formulated in a purely 3-dimensional context, we shall not be considering it further within the present work, based on purely one-dimensional simulations.

Despite their elegant formulation, kinetic theories based on mean field potentials have the drawback in lower dimensions of not fully capturing the large phase fluctuations in the quasi-condensate. In addition, so-called anomalous averages (or pair correlations) in the thermal cloud, typically omitted in such approaches, are expected to become particularly relevant at lower dimensions. It is not entirely clear, however, how to obtain a gapless excitation spectrum for the system in the homogeneous limit, as required by the Hugenholtz-Pines theorem [6, 7, 30–34]. A modified mean field theory for low-dimensional quasi-condensates was developed by Stoof’s group and one of the present co-authors [6, 7], building on previous path-integral approaches pioneered by Popov [3, 5]. In this “modified Popov theory”, the infrared divergences due to phase fluctuations are systematically removed, leading to a gapless, convergent and computationally convenient scheme that applies in all dimensions, for homogeneous and trapped systems. This approach has been used in particular to construct the phase diagram of weakly-interacting 1D systems [35], and to investigate the interplay of density and phase fluctuations [36].

The quasi-condensate dynamics at nonzero temperature is a challenging problem as the Bogoliubov approximation becomes invalid, at least at large times [37, 38], and large thermal phase fluctuations have to be taken into account even at low temperatures where density fluctuations are small [39]. Classical field methods have been developed to simulate numerically those modes of the system that feature a macroscopic occupation. These methods rely upon the observation that for highly occupied modes, the field operator can be replaced by a classical complex field which evolves in time according to the GPe [40–42]. This description extends the $T = 0$ GPe, by adding stochastic elements that describe fluctuations of the (quasi-)condensate modes; these may be further coupled to the thermal cloud where the mean occupation numbers are small. (In fact, too small to be treated in the classical field approximation, and more appropriately described by quantum Boltzmann equa-

tions [43].) Within the class of classical field techniques, we mention the projected GPe (pGPe) [41, 44], the truncated Wigner (tW) method [37, 45–47] the stochastic Gross-Pitaevskii equation (sGPe), when implemented in the classical limit [43, 48–53], and closely related classical field methods [42, 54]. Hybrid simulation techniques were also recently developed that attempt to go beyond the classical limit [55–58].

These stochastic approaches, the relation between them and other kinetic theories and their respective applications have been reviewed in Refs.[52, 53, 59, 60]. A key appeal is that they provide an approximation to the full distribution function of the ultracold gas and give access to physics beyond the mean field. They have been used, e.g., to probe the large critical fluctuations near the phase transition [61–63], to study dynamical effects of fluctuations on condensate growth [48, 49, 64] and macroscopic excitations [65–69]. Another quantity of interest is the counting statistics of the condensate mode [63, 70–73], which is analogous to the photon number distribution in quantum laser theory [74].

As the use of classical field simulations becomes more widespread, a quantitative study of their relative properties is essential. The main purpose of this paper is to initiate such a quantitative study by comparing two methods that can be implemented with reasonable effort, each of which generates an ensemble of stochastic initial states to mimic a finite-temperature Bose gas at equilibrium in a trap. For simplicity, we focus on a one-dimensional, weakly interacting system.

Number Conserving Bogoliubov (tWncB): The first method is a Bogoliubov approach in which the total atom number N is conserved (formulated within the canonical ensemble) [46, 77–81]. This method has been used as a starting point for dynamical calculations within the truncated Wigner approximation (see Ref.[60] for a review). We henceforth denote this by tWncB. The tWncB field contains both condensate and non-condensate modes, calculated from the Bogoliubov-de Gennes equations. The modes amplitudes are sampled to capture both quantum and thermal fluctuations. We adopt here a formulation developed in a low-temperature expansion around the Gross-Pitaevskii mean field [46, 80], assuming that N_{th} , the number of atoms in non-condensate modes, is small compared to N .

Stochastic Gross-Pitaevskii Equation (sGPe): The second method is the stochastic Gross-Pitaevskii equation (sGPe), which prepares a grand-canonical ensemble dynamically by simulating a Langevin equation (see Refs.[43, 48, 49] for details of the scheme used here). We consider it here within the classical approximation where the mode occupations are large. The stochastic field in the sGPe represents the low-lying modes of the field which are coupled to a thermal cloud, treated

as a heat bath. The exchange of particles and energy through incoherent scattering processes between these two sub-systems is represented by a damping term and the Langevin force in the sGPe [43].

We wish to show that there exist regimes where the two methods are equivalent despite the physically very different pictures behind them. To this end, we calculate and analyze relevant observables like density profiles, spatial correlation functions, and condensate statistics. Where feasible, we also compare to alternative finite temperature theories, as detailed in Table I. This study is by no means complete (e.g., there is no comparison to ‘ZNG’ or pGPe), but we believe that it represents an important step towards benchmarking commonly used simulation methods for finite-temperature Bose gases. Other comparisons undertaken to date are summarized in Ref.[82].

More specifically, we explain the origin of discrepancies between the two methods considered here, building on previous investigations of the validity conditions of the tWncB [38]. We find in particular that the low-temperature (or small N_{th}) expansion behind the tWncB breaks down quite early, as the temperature T increases towards the characteristic temperature T_ϕ for phase coherence within a trap [4]:

$$k_B T_\phi = N \frac{(\hbar\omega)^2}{\mu} < k_B T_c = \frac{N}{\ln 2N} \hbar\omega \quad (1)$$

(ω is the trap frequency and μ the chemical potential) where T_c is the critical temperature for Bose-Einstein condensation in an ideal trapped Bose gas in 1D [76]. This failure, that also happens when the theory of Ref.[71] is applied to an interacting, trapped gas, is attributed to a distribution function for N_{th} that is broadened by thermal fluctuations beyond the limit set by the total number of particles N . In addition, these fluctuations are overestimated because of spurious contributions from phase fluctuations. We have observed that the breakdown of the tWncB approach is not completely “cured” by propagating the stochastic ensemble of wave fields under the GPe.

At low temperatures and for smaller systems, we have found large number fluctuations in the sGPe results, in particular in the counting statistics of the condensate. This is related to the anomalous number fluctuations of the ideal gas in the grand-canonical ensemble [70, 83, 84]. This feature does not occur for the canonical tWncB method, and it is removed in larger condensates where particle interactions become important. We emphasize that this agreement illustrates how moments of the quantum field of very high order are correctly reproduced by the stochastic approaches.

In addition, we discuss the influence of the thermal (non-condensate) density $n_{\text{th}}(z)$ and the so-called anomalous average (or pair correlation) $m(z)$ of the

TEMPERATURE REGIME	PHYSICAL PROPERTY	SGPE	NCB	'BENCHMARK' THEORY FOR COMPARISON	REF.	SEC.
$T < T_\phi/2$	Density profiles: Total	✓	✓	modified Popov	[6, 7]	III A
	Density profiles: condensate (Penrose-Onsager)	✓	✓	modified Popov	[6, 7]	III B
	Spatial correlation function: 1 st order	✓	✓	modified Popov	[6, 7]	III C 1
				Petrov <i>et al.</i>	[4]	
	Spatial correlation function: 2 nd order	✓	✓	Kheruntsyan <i>et al.</i>	[75]	III C 2
	Condensate statistics	✓	✓	Svidzinsky and Scully	[71]	III D
$0 < T < T_c$	Pair anomalous average	✓	✓	($T = 0$) Bogoliubov theory	[1, 2]	III C 3
	Quasi-condensate/condensate density profiles	✓		modified Popov	[6, 7]	IV A

Table I: Summary of ‘benchmark’ theories used in analyzing the stochastic approaches. A tick in the ‘ncB’ or ‘sGPe’ columns indicates inclusion in the comparison. T_ϕ [Eq.(1)] is the critical temperature above which the system’s coherence length is smaller than its size due to phase fluctuations [4]. T_c [Eq.(1)] is the critical temperature for an ideal Bose gas in a one-dimensional harmonic trap [76]. These temperatures are illustrated in Fig.4 in relation to our parameters.

non-condensate field, by analyzing their back-action on the shape of the (Penrose-Onsager) condensate density. This anomalous average is related to both a renormalization of the particle interactions due to the background field, and to the Landau and Beliaev damping of condensate excitations (together with triple averages) [2, 7, 10, 11, 15, 32, 34, 81, 85–91].

Following on from this, we discuss the connection between the condensate mode, as obtained by applying the Penrose-Onsager criterion, and the quasi-condensate, as predicted by the modified Popov theory of Andersen *et al.* [6, 7]. In stochastic theories, the condensate mode is commonly extracted *a posteriori* from the total matter field ensemble, which can become a prohibitive computational task in large systems. This is in stark contrast to kinetic theories based on symmetry breaking, where the condensate is a separate quantity, obeying its own equation of motion. We extend the analysis of Ref.[92] to construct an approximate formula for the condensate density involving first- and second-order correlation functions which are straightforwardly obtained. This illustrates the conceptual difference between the Penrose-Onsager condensate and the quasi-condensate.

The paper is organized as follows: We first describe in Sec. II the procedure of initial state generation within each of the two selected stochastic approaches, highlighting the key conceptual differences between them. We also briefly review the modified Popov theory that is used to benchmark a number of our results. Sec. III addresses the equilibrium properties such as density profiles and correlation functions, comparing to other, pertinent theoretical results where appropriate. In Sec. III D, the condensate statistics is discussed and some features of the one-body density matrix in the quasi-condensate regime are illustrated. Sec. IV uses the modified Popov approach to address the physical mean-

ing of the (Penrose-Onsager) condensate mode, which may be extracted from the stochastic theories, and contrast this to the quasi-condensate concept. Sec. V shows that the ncB initial state under GPe evolution does not lead to improved predictions for equilibrium properties. Sec. VI summarizes our results, with some additional material presented in two appendices for completeness.

II. SIMULATION TECHNIQUES UNDER CONSIDERATION

Each of the stochastic simulation techniques we describe here are based on the mapping of a quantum field theory of atoms to noisy c-number fields. In this section we discuss them in turn, paying particular attention to two important practical elements: (i) the method of equilibrium initial state generation and (ii) the nature in which the GPe arises as an energy and number conserving means to treat the system dynamics away from equilibrium.

A. Truncated Wigner

In the truncated Wigner (tW) method, the temporal dynamics is governed by the familiar nonlinear Schrödinger or Gross-Pitaevskii equation (GPe):

$$i\hbar \frac{\partial \psi}{\partial t} = H_{\text{GP}}[|\psi|^2]\psi - \mu\psi, \quad (2)$$

$$H_{\text{GP}}[|\psi|^2] = -\frac{\hbar^2}{2m} \frac{\partial^2}{\partial z^2} + V(z) + g|\psi(z)|^2,$$

where the nonlinear Hamiltonian H_{GP} contains the trapping potential $V(z)$ and the effective two-body interaction strength g , and μ is the chemical potential. While Eq.(2) looks identical to the usual $T = 0$ GPe

equation, the meaning of ψ is quite distinct: (i) The complex field $\psi(z, t)$ represents the condensate, its elementary excitations, and the “thermal cloud” surrounding it. (ii) The initial conditions are stochastic and include quantum and thermal fluctuations of the condensate and its excitations. This is essential for incorporating spontaneous processes (scattering or decay) that are not captured within mean field theory, see, e.g. Ref.[93, 94]. (iii) Averages of operator products are first symmetrized before being mapped to classical fields, so that the one-body density matrix becomes, for example,

$$\langle \hat{\Psi}^\dagger(z) \hat{\Psi}(z') \rangle \mapsto \langle \psi^*(z) \psi(z') \rangle_W - n_q \delta_{z,z'} \quad (3)$$

where the average $\langle \dots \rangle_W$ is taken over the initial conditions. The second term is a δ -function on a spatial grid and proportional to the “quantum density”

$$n_q = \frac{1}{2\Delta z} \quad (4)$$

where Δz is the grid spacing. As a consequence of this “Wigner symmetrization”, the density in the nonlinear term in the Hamiltonian H_{GP} [Eq.(2)] should appear with a subtraction, $|\psi(z)|^2 - n_q$. We have incorporated the corresponding (small) energy shift gn_q into the chemical potential μ . (See, e.g. Ref.[95] how to generalize the mapping (3) to two-time correlations.)

B. Number conserving Bogoliubov initial state

To obtain a thermal initial state for use in the tW simulations, we employ a stochastic sampling for the canonical density operator at thermal equilibrium, based on the (number-conserving) Bogoliubov (ncB) approximation. In the usual Bogoliubov theory, one shifts the Bose field operator by a c-number field (the order parameter), which is equivalent to assuming that the system is in a superposition of states with different particle number (coherent state). The number-conserving version of the Bogoliubov theory [78, 79]. preserves the total number of atoms, N , and is constructed to provide the correct counting statistics for the condensate mode, in the limit of a small thermal component. (The distribution function $P(N_c)$ for the number of atoms in the condensate is discussed in Sec.III D.) Here, we summarize a practical scheme to sample the canonical equilibrium density operator for the quantum field at a fixed number of atoms N , as explained in Refs.[37, 46]; a number of technical details can be found in Appendix A.

1. Condensate mode

The initial value for the classical field $\psi(z, 0)$ is split as

$$\psi(z, 0) = a_c \phi_c(z) + \psi_\perp(z), \quad (5)$$

where the first term describes the condensate, a_c being the corresponding complex amplitude and $N_c = |a_c|^2$ the number of condensate atoms. The condensate mode function $\phi_c(z)$ is normalized to unity and is given in Eq.(A1). The splitting (5) is motivated from an expansion in the limits of large particle number N and small interaction constant g [78, 80, 81, 96]. More precisely, the condensate mode and its excitations are calculated self-consistently up to second order in $(N_{th}/N)^{1/2}$, where N_{th} is the number of non-condensed particles, respectively. (This number also has a small quantum contribution.)

2. Elementary excitations

The non-condensate field $\psi_\perp(z)$ in Eq.(5) arises in the next-order contribution of the ncB expansion. It is expanded in the basis of the Bogoliubov modes:

$$\psi_\perp(z) = \sum_k [b_k u_k(z) + b_k^* v_k^*(z)]. \quad (6)$$

The mode functions are the eigenvectors $(u_k, v_k)^T$ to the eigenvalue E_k of the Bogoliubov-de Gennes operator \mathcal{L}_Q given in Eq.(A3). The Bogoliubov spectrum $\{E_k\}$ is positive and gives the quasi-particle energies relative to the chemical potential. The Bogoliubov amplitudes b_k, b_k^* in Eq.(6) are sampled as independent complex Gaussian random numbers with zero mean and variance $\sigma_k^2 = (1/2) \coth(\beta E_k/2)$ [37, 38]. The mean population of a Bogoliubov mode is thus equal to

$$\langle |b_k|^2 \rangle_W = \sigma_k^2 = \bar{N}(E_k) + \frac{1}{2}, \quad (7)$$

the Bose-Einstein occupation number $\bar{N}(E_k)$ plus an extra contribution $1/2$. This extra term appears due to the symmetric ordering of the quantum operators:

$$\langle |b_k|^2 \rangle_W \leftarrow \frac{1}{2} \langle b_k^\dagger b_k + b_k b_k^\dagger \rangle, \quad (8)$$

and represents quantum fluctuations. Quantum fluctuations mimic spontaneous scattering into otherwise empty modes within a classical field approximation [53]. They also lead to the depletion of the condensate mode [97]. The condensate mode function $\phi_c(z)$, indeed, contains a correction that depends on these amplitudes [the field $\phi_2(z)$ discussed after Eq.(A8)]. Within the number-conserving scheme of Ref.[38], this correction reflects the change in the condensate number (quantum and thermal depletion), the interaction between condensate and non-condensate particles via the Hartree-Fock potential $2g\langle |\psi_\perp(z)|^2 \rangle_W$ and via the anomalous average $g\langle (\psi_\perp(z))^2 \rangle_W$, see Eqs.(A9, A10).

3. Condensate number

The stochastic ensemble of the non-condensate fields $\psi_{\perp}(z)$ now determines the sampling of the condensate number. The number of condensed atoms N_c is calculated from [37, 38]

$$N_c = N - N_{\text{th}}(\{b_k\}) + \mathcal{A}(\{b_k\}), \quad (9)$$

$$N_{\text{th}}(\{b_k\}) = \Delta z \sum_z |\psi_{\perp}(z)|^2 - \mathcal{M}/2. \quad (10)$$

Here, N_{th} gives the number of non-condensed atoms, while \mathcal{M} is the number of terms in the expansion (6) and depends on the computational grid, and acts so as to subtract the “one half atom per mode” from the quantum fluctuations in ψ_{\perp} . The quantity $\mathcal{A}(\{b_k\})$, given in Eq.(A7), averages to zero and implements the “canonical constraint” at the level of variances: it ensures that the fluctuations of the condensate number N_c are anti-correlated to those of N_{th} (calculated in normal order), since the two number operators sum to the fixed total particle number N . Once N_c is calculated for each member of the ensemble, the condensate amplitude a_c in Eq.(5) is taken as $a_c = \sqrt{N_c}$. The global phase is arbitrarily fixed here but the ncB construction is actually U(1)-invariant (see endnote [137]), and the phase drops out in our observables of interest. A typical example for a Wigner field is given in Fig.1.

4. Validity range

We summarize a few issues that have to be considered for the initial state preparation within the ncB expansion and the tW scheme. There are two aspects here: First, the truncation made in order to obtain the evolution equation (2) assumes that third derivatives of the Wigner functional for the quantum field are negligible [37, 45, 53]. This should be the case when the total number of particles is much larger than the number of relevant modes in the simulation, i.e. $N \gg \mathcal{M}$. Given this restriction, however, the tW scheme gives approximate physical results even beyond the time scale where the Bogoliubov theory, in its number-conserving form, fails [37].

The second aspect is related to the low-temperature expansion of the number-conserving Bogoliubov approach that is behind the initial state preparation [37, 38, 46]. The canonical distribution of the Bose gas is calculated by approximating the Hamiltonian of the quantum field theory by the quadratic Bogoliubov Hamiltonian (as also done in Refs.[71, 98]). This is valid when the number of non-condensate particles is small: $N_{\text{th}} \ll N$ which implies relatively low temperatures. The sampling of the condensate statistics, Eq.(9), is also an approximation that has been discussed in Ref.[37]: in the

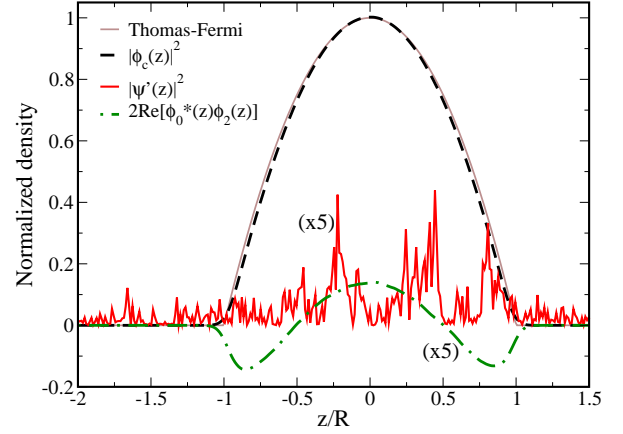


Figure 1: (Color online) Condensate density $N_c |\phi_c(x)|^2$ (dashed, black) and a typical realization of the non-condensate density $|\psi'(x)|^2 \equiv |\psi_{\perp}(x)|^2$ (noisy red curve; data is multiplied by 5 to be visible on this scale). The depletion correction to the condensate mode, $\phi_2(z)$, is illustrated by plotting the ‘interference term’ $2 \text{Re}[\phi_0^*(x)\phi_2(z)]$ (dot-dashed, green; also multiplied by 5). Note that the condensate atom number $N_c \approx 19500$ depends on the realization. The zero-temperature Thomas-Fermi shape for the same parameters (inverted parabola; thin, solid brown line) is also plotted. Here (and in most of the paper) we fix $\mu = 22.41 \hbar\omega$ (corresponding to $N = 20000$ for the GPe at $T = 0$), choosing here $k_B T = 46 \hbar\omega$. Densities are plotted in units of g/μ .

quantum field theory, N_c is restricted to be an integer (eigenvalue of the number operator $\hat{a}_c^\dagger \hat{a}_c$), while the classical simulation returns continuous values for N_c . Both schemes coincide when the counting statistics $P(N_c | \psi_{\perp})$ (conditioned on a given non-condensate field ψ_{\perp}) is broad enough, and can be extended to a smooth function of N_c . It has been shown that this condition can be met when ψ_{\perp} is sampled with sufficiently many modes (\mathcal{M}_{th} , say) having a significant thermal occupation (see [38] for more details). For a typical mode spacing $\hbar\omega$, this gives a lower limit on the temperature because we need $\mathcal{M}_{\text{th}} \equiv k_B T / (\hbar\omega) \gg 1$. Under these conditions, one can also justify the gaussian probability distribution for the non-condensate field ψ_{\perp} that is used in the simulation scheme [38].

In summary: since the Bogoliubov approximation is used for the representation of the N -body density operator, the temperature should be not too high but at the same time also not too low because of the smoothness of the distribution function. This poses limits on the applicability of the state preparation protocol within tWncB. The above requirements can be checked from the inequalities [37]

$$\mathcal{M}_{\text{th}} \leq \langle N_{\text{th}} \rangle \ll \sigma^2(N_c) \quad (11)$$

where $\sigma^2(N_c)$ is the variance of the (unconditional) condensate statistics $P(N_c)$, obtained from the sampling (9).

The first inequality precludes very low temperatures because N_{th} would be too small. In addition, the condensate statistics must not be too broad,

$$\sigma(N_c) \ll \langle N_c \rangle = N - \langle N_{\text{th}} \rangle \quad (12)$$

because otherwise the probability of returning negative values for N_c would become significant. The method gives unphysical results if a large fraction of negative values of N_c is returned and we find that this happens already at moderate temperatures, when $\langle N_{\text{th}} \rangle / N$ becomes of the order of ~ 0.2 .

C. Stochastic Gross-Pitaevskii equation

Within the stochastic Gross-Pitaevskii equation, a finite temperature equilibrium state is obtained dynamically by evolving a complex field $\psi(z, t)$ that is coupled to a thermal cloud which, when approximated as in thermal equilibrium, acts as a heat bath (energy and particle reservoir) [43, 48, 51, 53, 99].

1. System plus bath split

We may physically motivate a division into two subsystems: the system is represented by the field $\psi(z, t)$ and describes the low-lying modes of the ultracold gas. These are highly occupied, therefore a classical field description is appropriate; the “thermal cloud” of atoms whose energies are high above the typical energies of the condensate and its excitations, obeys a separate quantum Boltzmann equation [43]. Both subsystems are naturally coupled to each other by exchanging energy and particles, hence the description is given within the grand-canonical ensemble. This leads to a nonlinear Langevin equation (see Eq.(13)), often termed the stochastic GPe (sGPe). The system dynamics now combines deterministic aspects (encapsulated within the usual GPe) and a stochastic coupling to the heat and particle reservoir of thermal atoms.

We note that there are two distinct formulations of such a nonlinear Langevin equation, which are motivated by the same physical ideas, but which arise from very different formalisms (see Ref.[52] for a review and a discussion of subtle differences). The derivation of Stoof, which we shall adopt in this work, is based on the Keldysh non-equilibrium formalism [43, 49, 100] and the resulting theory was first implemented numerically in Ref.[48]. An equation that differs in some details was formulated by Gardiner, Anglin and Fudge [50] and cast into its current form by Gardiner and Davis [51], as a limiting case of the quantum kinetic theory put forward by Gardiner and Zoller [18, 101, 102]. The stochastic equation which results, differs primarily in the use

of a projector operator restricting dynamics to low energy modes, and is termed the stochastic projected GPe (spGPe) [53].

Technically, the particular sGPe discussed here is obtained by expanding the system density matrix over coherent states using functional integration techniques, which leads naturally to the Keldysh non-equilibrium formalism. Ultimately, this is found to give a Fokker-Planck equation for the Wigner distribution function of the entire atomic quantum field [100, 103]. This procedure maps symmetrically ordered correlation functions of field operators onto stochastic field correlations, as is evident from the fact that each mode k of the classical field ψ occurs in the stationary limit with an occupation number $\bar{N}(E_k) + 1/2$ [43, 60] (cf. also Eq.(7)). Within the modes which are predominantly classical, i.e. highly occupied, $\bar{N}(E_k) \gg 1/2$, and this symmetrization is no longer important, a common consideration in *all* classical field methods [40–42, 53]. This approximation will permit us to move from the quantum relation Eq. (14) below to its classical counterpart Eq. (15) which makes the simulation scheme much simpler.

2. Stochastic equation of motion

Making a Hartree-Fock type *Ansatz* for the probability distribution representing the entire trapped gas, leads to two separate probability distributions, representing separately the high- and low-lying system modes. Integrating out the low-energy modes, one finds that the former may be treated by a quantum Boltzmann equation (qBe) [43]. Integrating instead over the high-energy modes leads to a nonlinear Langevin equation,

$$i\hbar \frac{\partial \psi}{\partial t} = \left(H_{\text{GP}}[|\psi|^2] - \mu - i\hat{R}(z, t) \right) \psi + \eta(z, t), \quad (13)$$

where $\hat{R}(z, t)$ is a damping term, which should in general be time dependent, and $\eta(z, t)$ a stochastic “force”. Note that it is for convenience in later discussions only that we use the same symbol for the tWncB and sGPe wavefunctions, despite the differences in physical content. Assuming that the dynamics of the high-energy modes may be neglected, the physical picture underlying this equation is a splitting of the quantum field into low-lying modes (the “system”, described by $\psi(z, t)$) and a “thermal particle bath”, which is considered to be at equilibrium and so, on average, Bose-Einstein distributed [49] (since this is the equilibrium solution to the qBe). The term $-i\hat{R}(z, t)\psi(z, t)$ describes the particle exchange due to collisions between system and bath atoms. The real part of the operator \hat{R} can be positive or negative, corresponding to loss or growth, as for the analogous operator appearing in the ZNG scheme [22]. Since collisions occur randomly, the sGPe contains an

associated ‘noise’ term $\eta(z, t)$ in Eq.(13). The presence of both terms, dissipation and noise, is essential to ensure that the fluctuation-dissipation theorem is satisfied: the system is thus guaranteed to reach the correct equilibrium at a given temperature.

3. Damping and noise

The damping operator is given by the relation

$$-i\hat{R} = \frac{\hbar\Sigma^K}{4} (\bar{N}(\hat{\epsilon}_c - \mu) + 1/2)^{-1} \quad (14)$$

where $\hbar\Sigma^K$ is the so-called Keldysh self-energy (a complex quantity) and $\bar{N}(\epsilon_c - \mu)$ is the Bose-Einstein distribution, representing the occupation of low-lying modes as a function of mode energy ϵ_c . While this relation is exact at equilibrium, it cannot be easily implemented in this form in numerical simulations for the following reasons: firstly, the mode energy $\hat{\epsilon}_c$ actually corresponds to the nonlinear differential operator appearing in the GPe (13); moreover, Σ^K is determined by the thermal particle distribution, whose accurate temporal representation would require solving a qBe. We therefore restrict the sGPe to its classical limit, as *all* current numerical applications of this theory do. In the approach of Stoof, this means that the action of the damping operator takes the simple form

$$-i\hat{R}\psi = \frac{\hbar\Sigma^K}{4k_B T} (H_{\text{GP}}[|\psi|^2] - \mu) \psi. \quad (15)$$

where $\hbar\Sigma^K$ is still spatially dependent in general [49, 66], as the thermal particle energies are affected by the condensate mean-field. This enables the equation to be cast in the form

$$i\hbar \frac{\partial \psi}{\partial t} = (1 - i\gamma) \left(H_{\text{GP}}[|\psi|^2] - \mu \right) \psi + \eta(z, t), \quad (16)$$

where $\gamma = i\hbar\Sigma^K/4k_B T$. The *form* of this equation is the same as the stochastic pGPe (spGPe) implemented numerically by Davis and collaborators, except for the projector [53] (see Ref.[52] for a more detailed comparison).

In Eq.(16), the term $\eta(z, t)$ is a complex, Gaussian, white-noise process with correlations

$$\langle \eta^*(z, t) \eta(z', t') \rangle = 2\hbar\gamma k_B T \delta(t - t') \delta(z - z'). \quad (17)$$

This relation can be read as a fluctuation-dissipation theorem for the system, since the strength of fluctuations is proportional to the damping parameter γ , on the one hand, and the temperature T of the heat bath, on the other. This link is essential for the preparation of a thermalized system. A similar stochastic scheme was formulated in Ref.[57] for the ideal Bose gas where the

noise was filtered in order to preserve the total atom number (canonical ensemble).

Since our primary interest in the present work is in generating an ensemble of equilibrium states, we make a further, numerically convenient, simplification and treat Σ^K as a parameter independent of time and, additionally, space. This is also a standard approximation in spGPe simulations [53], and we have tested that a spatially varying Σ^K does not strongly affect the equilibrium state. So, for our present purposes, we solve Eq. (16) with the dimensionless quantity $\gamma = 0.01$.

4. Validity range

The main limitation behind the sGPe used here is the classical approximation (highly occupied modes), as highlighted by the relation (15). In the case of a trapped system, this means that the applicability of the theory varies spatially. Indeed, the classical approximation is better suited to the low energy, central region of the trap, in which there are many particles due to the presence of a Bose-Einstein condensate. In the outer trap regions, there are fewer atoms, and hence there comes a point beyond which the classical approach is no longer well justified. In general, this point is dependent upon the choice of grid spacing, as a finer grid includes more high-energy modes. For a given grid with spacing Δz , the accuracy of the classical approximation can be checked by comparing, for example, the average density $\langle |\psi(z)|^2 \rangle$ to the quantum density $n_q = (2\Delta z)^{-1}$ (this value arises from operator symmetrization in Eq.(3) on the grid). We shall see that this limits the applicability of the classical approximation to the sGPe typically to the spatial range where the trapping potential is not too large, $V(z) - \mu \leq k_B T$. Within this study, we are interested primarily in the central region $|z| < R$ where the condensate is present (R is the Thomas-Fermi radius), as also highlighted in the original sGPe numerical implementation [48]. We have verified that changes in the properties which form the basis of our comparison are negligible over a range of grid spacings. This is physically equivalent to the statement that our equilibrium results are unchanged for a range of cutoff energies, which mark the split between the low- (‘classical’) and high-lying (‘thermal’) modes (see also Refs.[44, 53, 99, 104]).

5. State preparation

We now briefly explain how the sGPe (16) works in practice – more details on this can be found in recent reviews [53, 99, 104]. As initial condition for the system, one can start with $\psi(z, 0) \equiv 0$. The dissipative term $-i\gamma$ in Eq.(16), leads to a change in the norm of $\psi(z, t)$,

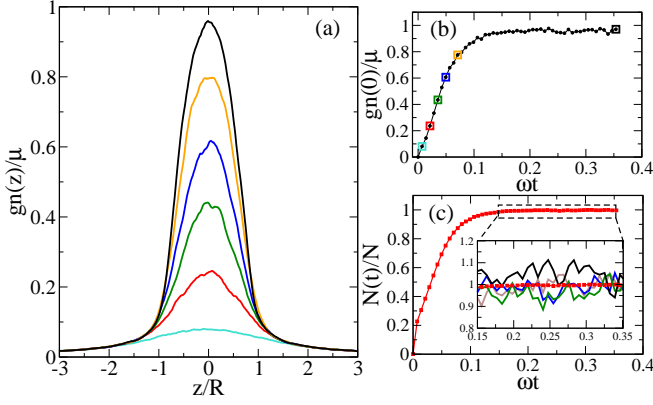


Figure 2: (Color online) Growth to equilibrium obtained by numerical solution to the sGPe. (a) Snapshots of the atomic density profile $\langle |\psi(z, t)|^2 \rangle$, with time increasing from bottom to top. (b) Growth in the average central density vs. time – here the times highlighted by colored squares label the corresponding colored density profiles in (a). (c) Growth in the particle number as the system approaches equilibrium. The inset shows trajectories from single numerical realizations, which illustrates the fluctuating particle number between these, compared to the result of the main plot in (c), which was obtained by averaging over 1000 such trajectories. (Parameters: as stated in subsection II F, but with $k_B T = 860 \hbar \omega$.)

but this cannot increase a zero initial condition. It is the Langevin force $\eta(z, t)$ that ‘seeds’ the field, as discussed in [48]. The particle number $N(t) = \sum_i \Delta z |\psi(z_i)|^2$ increases until $\psi(z, t)$ relaxes to the solution of the stationary GPe, at a given chemical potential

$$H_{\text{GP}}[|\psi|^2]\psi = \mu\psi, \quad (18)$$

as illustrated in Fig.2. The state preparation in the sGPe is thus performed *dynamically*, as the system grows to equilibrium in contact with a heat bath at a specified temperature. Once the dynamical equilibrium is reached, the presence of the noise term $\eta(z, t)$ ensures that $N(t)$ fluctuates about its final value. The final, average atom number $\langle N \rangle$ depends on the heat bath parameters (temperature T , chemical potential μ), on the trap parameters and the atomic species (through the interaction constant g). Although the subsequent dynamical evolution requires these noise terms to be maintained, a simpler scheme, bearing close analogies to the truncated Wigner method, can be based on dynamical propagation of the sGPe equilibrium state via the GPe; such an approach was first implemented in [64] to discuss quasi-condensate growth on an atom chip.

It is clear that in the grand-canonical ensemble, N has a statistical distribution of non-zero width; this width is related in the case of the sGPe to the ‘history’ of the particle transfer between system and heat bath as modelled by the Langevin seed $\eta(z, t)$. In the simulations, we observe indeed that N differs quite substantially from real-

isation to realisation, however the equilibrium value is obtained with reasonable accuracy after averaging over a few hundred of them. The temporal variations in the ensemble-averaged particle number then become relatively suppressed. For smoother results and for improved accuracy, all results presented in this work are based on a sample of at least 1000 individual realisations.

D. Linking the theories

At $T = 0$, the Gross-Pitaevskii equation represents the dynamics of a Bose-Einstein condensate by treating the system as made up of a single, coherent mode. Within the tW approach, the GPe is instead used to propagate a multi-mode system, the initial conditions being chosen at random to sample the initial density operator of the system. The ensemble of wave functions $\psi(x, t)$ represents *all* modes of the matter wave field, within the limits set numerically by the spatial grid, which physically corresponds to the energy cut-off choice for the modes being probed. It is for this reason that no explicit noise terms (Langevin forces) appear, and that the total number of atoms (the norm of $\psi(x, t)$) is conserved. The initial mode amplitudes combine quantum and thermal effects [see Eq.(7)] consistent with the Wigner mapping to symmetrically ordered operator products. Polkovnikov has shown that the truncated Wigner approximation captures the next order correction beyond Gross-Pitaevskii in an expansion in \hbar [47]. The initial state that we prepare here is based on a fixed number of atoms N (canonical ensemble), using the number-conserving Bogoliubov approach, although alternative (grand-canonical) schemes could be adopted as well [53]. Once we focus on low-lying modes, like the condensate mode, we recover nevertheless a broad distribution for the non-condensed atoms N_{th} (the mirror image of the condensate statistics $P(N_c)$). In this perspective, we can even consider μ in Eq.(2) as a “chemical potential” for the Bogoliubov modes: the condensate plays the role of a particle reservoir, as is perfectly reasonable if its population is large [105].

In the sGPe approach, the wave function $\psi(z, t)$ represents instead the low-lying modes of the system; although higher-lying modes should in principle be described by a quantum Boltzmann equation, here they are assumed to remain at equilibrium, thereby providing a heat bath to the low-energy sub-system under consideration. In the Bose-condensed phase, low lying system modes are highly occupied and the classical approximation, amounting to replacing the Bose-Einstein by the Rayleigh-Jeans distribution, is well justified. The dynamics of the low-lying modes is quite different, however, because particle exchange with the bath is allowed

for; this method is therefore a grand-canonical one, as can be seen by the growth plots of Fig.2. The “system-bath split” can be applied to a trapped gas (a closed system) by choosing modes below a suitably small cutoff. For a fully self-consistent calculation, in which the thermal cloud dynamics are also accounted for, this cutoff should be not lower than the global chemical potential [43]. For a classical field method not taking the entire thermal cloud dynamics into account, this should be chosen such that the highest modes simulated are macroscopically occupied [53]. It has been proposed that a cutoff equal to $k_B T$ yields optimum results for the condensate statistics of an ideal gas [106]. For the purposes of our comparison, we have adopted a different choice here, and have taken for consistency the same spatial grid in the sGPe and the tWncB simulations, which gives a cutoff of the order of $E_{\max} \sim \hbar^2/(m\Delta z^2)$.

Let us summarize the differences between the initial state ensembles of the two methods:

- (1) The total atom number N fluctuates in the sGPe (grand-canonical), and is fixed in tWncB (canonical).
- (2) The system is thermalized either dynamically (sGPe) by weakly coupling it to a heat bath, or by populating its excitation modes with thermal statistics (tWncB). Low-lying thermal modes above the condensate equilibrate under the sGPe to the Rayleigh-Jeans statistics (classical equipartition). This is actually the equilibrium distribution for the finite temperature GPe, considered as a classical field equation, as has been seen by studying thermalization in related classical field methods [40–42]. Within the tWncB scheme, these modes are populated according to the usual Bose-Einstein statistics, with the addition of $1/2$ “quantum atom” per mode. This coincides well with the Rayleigh-Jeans statistics for modes with energies below $k_B T$ [107], but gives a larger contribution to high-energy modes, up to the numerical cutoff. The tW dynamics under the GPe redistributes these “quantum atoms” with the others, leading, by the equipartition law, to an effectively higher temperature. This restricts applications of the tW scheme to relatively short simulation times. In nearly integrable systems (like the quasi-one-dimensional gas), thermalization can be quite slow, however [108, 109].
- (3) The energy spectrum of the elementary excitations is calculated in tWncB approximately, ignoring the thermal depletion of the condensate. Indeed, the Bogoliubov-de Gennes operator [Eq.(A4)] assumes that all particles are in the condensate mode.

E. Modified Popov theory

1. Motivation

While the stochastic approaches discussed thus far are suitable to describe both non-equilibrium and static properties of the Bose gas, we focus in this study on the detailed analysis of a partially condensed Bose gas at thermal equilibrium. Mean field theories [52] are often applied to study the thermodynamics in higher-dimensional Bose systems, and their solution is, in general, less involved than with stochastic theories. In comparing the equilibrium properties of the sGPe and ncB approaches, it will therefore prove useful to have an independent method for comparison.

In lower dimensions, mean field theories have to cope with infrared divergences due to the enhanced role of fluctuations, as predicted within the Mermin-Hohenberg-Wagner theorem [110, 111]. The Popov approach [3] where the fluctuations are split into phase and density contributions, has proven useful to treat phase fluctuations in low dimensions beyond second order around the mean field. A consistent regularization scheme has been developed in the modified Popov theory of Andersen *et al.* [6, 7, 112], extending the work of Petrov *et al.* [4] and Kagan *et al.* [5]. The resulting formulas apply to any temperature and dimension, while simultaneously being relatively straightforward to solve.

2. Quasi-condensate density

In low dimensions, a condensate does not arise in a homogeneous system, but still there is a temperature range $T_\phi \sim T < T_c$ where a so-called quasi-condensate can be identified whose density fluctuations are suppressed [3–7]. In the modified Popov theory, the quasi-condensate density n_{qc} may be obtained by solving self-consistently the following equations for the total density [Eq.(4) from Ref.[6]]

$$n = n_{qc} + \frac{1}{V} \sum_p \left[\bar{N}(E_p) \frac{\epsilon_p}{E_p} + \frac{\epsilon_p - E_p}{2E_p} + \frac{gn_{qc}}{2\epsilon_p + 2\mu} \right], \quad (19)$$

and for the chemical potential

$$\mu = g(2n - n_{qc}). \quad (20)$$

Here, $E_p = [\epsilon_p^2 + 2gn_{qc}\epsilon_p]^{1/2}$ is the Bogoliubov dispersion relation, $\epsilon_p = p^2/2m$, V is the system volume, and g denotes the two-body T-matrix (evaluated at -2μ , which corresponds to the energy cost of exciting two atoms from the condensate). Eq.(19) is evaluated numerically, replacing the sums over momenta by an integral. (For

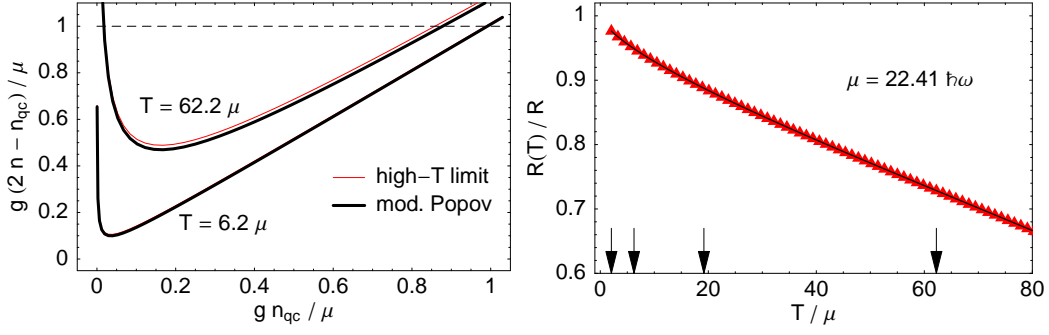


Figure 3: (Color online) Illustration of the procedure for solving the modified Popov theory. (left) Graphical determination of the self-consistent quasi-condensate density: crossing point between the dashed and solid lines (lhs and rhs of Eq.(20), n_{qc} is the quasi-condensate density and n the total density). Thin (red) line: classical (high-temperature) approximation to Eq.(19). If we take μ as in the rest of the paper, the two temperatures correspond to $N \approx 23\,800$, $T \approx 1.3 T_\phi \approx 0.63 T_c$ and $N = 20\,000$, $T \approx 0.16 T_\phi \approx 0.074 T_c$, respectively (see Eq.(1)). (right) Temperature-dependent Thomas-Fermi radius $R(T)$ determined by numerically solving for the (local) chemical potential where $\mu(z) = 2gn'_{th}(z)$. The trap is harmonic, chemical potential at the center $\mu = 22.41 \hbar\omega$ as in the rest of the paper, and $g = 0.01 (\hbar^3\omega/m)^{1/2}$. The arrows mark the temperatures chosen for the simulations [Table II].

a link with conventional mean field theories see Sec. III B 2).

Eqs. (19) and (20) can also be applied in a trap within a local density approximation, using a local chemical potential $\mu(z) = \mu - V(z)$. The quasi-condensate density is then found by solving [Eq.(54) of Ref.[7]]

$$(H_{GP}[n_{qc}] + 2gn'_{th}(z)) \sqrt{n_{qc}(z)} = \mu \sqrt{n_{qc}(z)} \quad (21)$$

where $2gn'_{th}(z) = 2g(n(z) - n_{qc}(z))$ is the Hartree-Fock potential due to the non-quasi-condensate particles. The spatial point at which $2gn'_{th}(z) = \mu(z)$ defines the temperature-dependent Thomas-Fermi radius, $R(T)$, that gives an estimate for the thermal depletion of the (quasi-)condensate (see Secs. III C 1, IV). We emphasize that this quantity is determined self-consistently within the modified Popov theory. For $|z| > R(T)$, we have $n_{qc}(z) = 0$, and adopting again the local density approximation, the atomic density corresponds to a thermal gas with a Hartree-Fock interaction,

$$n(z) = \int \frac{dp}{2\pi\hbar} \bar{N}(\varepsilon_{HF}(p, z) - \mu), \quad (22)$$

$$\varepsilon_{HF}(p, z) = \epsilon_p + V(z) + 2gn(z).$$

This procedure is illustrated in Fig.3 where the left panel shows both sides of Eq.(20) as a function of the quasi-condensate density n_{qc} . The crossing with the dashed line determines the self-consistent $n_{qc}(\mu, T)$. The (local) chemical potential can be lowered, which corresponds to moving further from the trap centre, until a minimum $\mu_{min}(T)$ below which the solution $n_{qc} = 0$ must be taken [35]. This defines the temperature-dependent Thomas-Fermi radius,

$$\mu \left(1 - \frac{R^2(T)}{R^2} \right) = \mu_{min}(T) \quad (23)$$

The right panel shows $R(T)$ in the temperature range of interest here: the quasi-condensate is shrinking smoothly and is about 20% smaller at $T \sim T_\phi$. (This number applies to the parameters introduced in Sec.II F.)

We recall that the central object within the modified Popov theory is the quasi-condensate, but this may be linked to the ‘true’ condensate (if it exists, as defined by the Penrose-Onsager criterion), as is discussed in Sec. IV. We will employ this modified Popov scheme in order to compare to various equilibrium properties where appropriate. This has the advantages of simplicity and speed over the stochastic approaches, due to the relatively straightforward manner in which the above equations may be solved.

F. Parameter choice for comparison

We wish to address the following issues:

- (i) Initial state generation: how does the finite-temperature initial state compare within each method?
- (ii) Ensemble choice: what role does the choice of thermodynamic ensemble play?
- (iii) How does the quasi-condensate and condensate extracted from the stochastic approaches compare to analogous quantities within the modified Popov theory?

Our focus being on the relative merits of the stochastic methods as thermal field theories, we choose to work in a regime in which thermal effects dominate over quantum effects. We consider a quasi-one-dimensional confinement with a trap frequency ω (oscillator length ℓ) and take an effective coupling constant $g = 0.01 \hbar\omega \ell$ which corresponds to the weakly interacting regime. We choose an (average) particle number, $N = 20\,000$, giv-

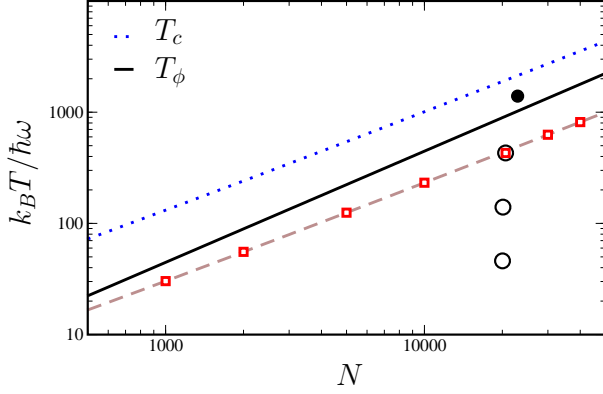


Figure 4: (Color online) Characteristic temperatures and atom numbers of the sGPe and ncB simulations (hollow black circles). The filled black circle shows the higher temperature regime at which only sGPe simulations were undertaken. The (1d) characteristic temperatures in a trap are T_c [Eq.(1); Bose-Einstein condensation in an ideal gas] and $T_\phi < T_c$ [Eq.(1); phase coherence], shown by the dotted blue and solid black lines respectively. The red squares mark the parameters chosen for the condensate statistics comparison of Sec.III D 1 at a fixed ratio $T/T_c = 0.23$, as indicated by the dashed brown line.

ing a chemical potential $\mu = 22.41 \hbar \omega$ for the ground state of the GPe. Within the sGPe, the chemical potential is kept fixed as temperature is varied, leading to a small variation in the particle number; this is however below 6% for the three temperatures at which we undertake the comparison. These are placed in context in Fig.4. In particular, we probe at the lowest temperature a regime well suited to tWncB due to the requirement that $N_{\text{th}} \ll N$, an intermediate regime, and a higher temperature in which the ‘classical’ sGPe is expected to be most appropriate, due to the occurrence of more highly populated modes. These are highlighted in Table II, also showing some other simulation parameters.

	$k_B T / \hbar \omega$	T/T_ϕ	T/T_c	L/R	\mathcal{M}	$\Delta z/\ell$
(a) low T	46	0.052	0.025	4.20	127	0.22
(b) interm T	140	0.16	0.074	12.0	1023	0.078
(c) high T	430	0.48	0.23	17.0	2047	0.055

Table II: Simulation parameters: Atom number and chemical potential are fixed to $N \approx 20\,000$, $\mu = 22.41 \hbar \omega$, with the characteristic temperatures T_c and T_ϕ as in Eq.(1). The computational grid covers $z = -L/2 \dots +L/2$, with spacing Δz , number of points \mathcal{M} . R is the Thomas-Fermi radius of Eq.(24) and ℓ the size of the single-particle ground state.

Length scales in the problem are scaled to the zero temperature Thomas-Fermi radius,

$$R = \sqrt{\frac{2\mu}{\hbar \omega}} \ell \approx 6.69 \ell. \quad (24)$$

Another relevant length scale is $z_T = \sqrt{2(k_B T + \mu)/\hbar \omega} \ell$, which marks the boundary at which the thermal energy becomes comparable to the trap energy. We take a grid size $L > 2z_T$ [Table II] and a spacing $\Delta z/\ell = \sqrt{2\pi/(\mathcal{M}+1)}$. The number of grid points, $\mathcal{M} + 1 = L/\Delta z$, is increasing with temperature in order to resolve the thermal wavelength $\lambda_T = \sqrt{2\pi\hbar/k_B T}$. The grid spacing is chosen such that for an ideal gas, the tWncB approach returns the correct total particle number $\langle N \rangle$. In addition, we check in the interacting case that doubling \mathcal{M} does not change $\langle N \rangle$. For time evolution via the (s)GPe, we use a Crank-Nicholson approach, and a fixed time step $\omega \Delta t = 10^{-4}$. Ensemble averages are performed over at least 1000 noise realizations.

A typical result of the stochastic methods is given in Fig.5 where the data points give the realizations for the complex field $\psi(z)$ at selected values of position z and temperature. The globally random phase of the sGPe data is quite obvious, from the spread around the circle, while the ncB ensemble fixes the condensate mode to have a real and positive amplitude. The overestimation of density fluctuations is also quite visible in the ncB data at intermediate and high temperatures, shown by the increased variation in the radius of the data points. Outside the condensate region (Thomas-Fermi radius R), there are no significant differences between either method, where the wavefunction represents an incoherent thermal gas.

III. EQUILIBRIUM PROPERTIES

We present here an analysis of the initial states produced by the two stochastic methods, that are expected to represent thermal equilibrium in the trap. The accuracy of this equilibrium state is important for modelling the finite-temperature dynamics when perturbations take the system far away from equilibrium, e.g., changes in the trapping potential.

A. Density profile

We begin with the total density profile $n(z)$. Similar to experimental data, this contains both the condensate in the trap center and thermally excited atoms that surround it. The equilibrium densities in a harmonic trap are plotted in Fig.6. Here and in the following figures, the sGPe densities (solid black) are calculated as $n(z) = \langle |\psi(z, t_{\text{eq}})|^2 \rangle$ where t_{eq} is the preparation time required for the system to reach a dynamical equilibrium with the bath. In the ncB data (dashed red), we subtract the ‘‘quantum density’’ $n_q = 1/(2\Delta z)$ according to Eq.(A12). This correction is small if the number of atoms

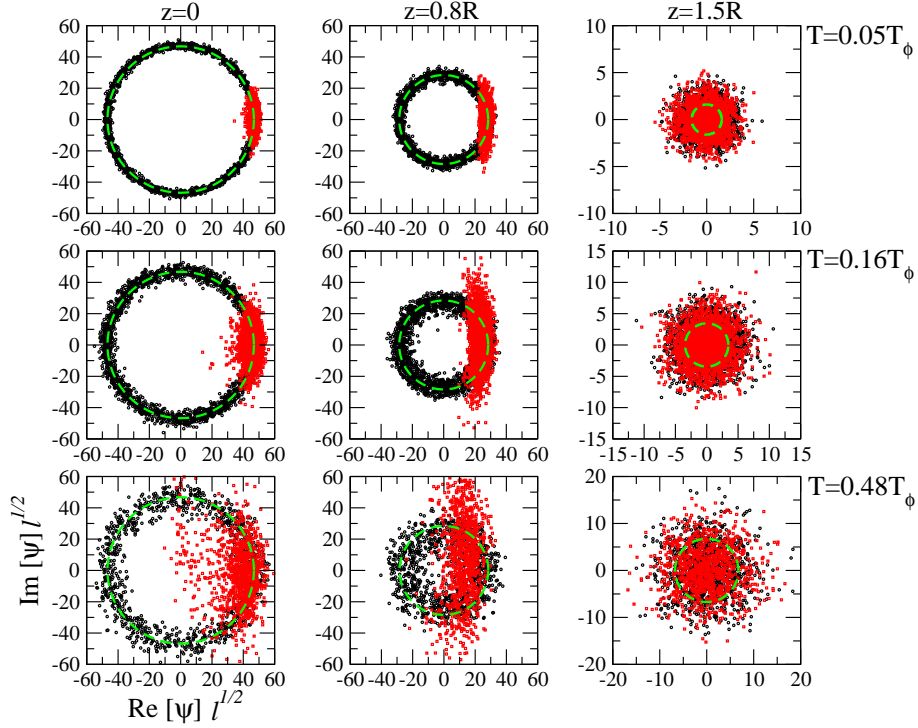


Figure 5: (Color online) Data points representing the ensemble of stochastic field values $\psi(z)$ at three positions z in the trap (from left to right, the average density decreases). Temperature increases from top to bottom. Black: sGPe simulation, red: ncB simulation. The dashed green circle indicates, for $|z| < R$, the modulus of the Thomas-Fermi wavefunction, and for $z = 1.5R$ the square root of the Bose-Einstein density (26). In the trap center, the Thomas-Fermi approximation yields for these parameters $|\psi_{\text{TF}}(0)| \approx 47/\sqrt{\ell}$. (Atom number $N \approx 20\,000$.)

per grid cell is large. In addition, its impact on the mean field is small since $gn_q \sim (1 \dots 4) \times 10^{-3} \mu$.

For an independent benchmarking, the total density profiles are also compared to the total density of the modified Popov scheme (green, dot-dashed). At the low and intermediate temperature regimes, we find good agreement between all three theories. At the higher T , Fig.6(c), the ncB result deviates from both the sGPe and modified Popov density profiles (which are found to agree perfectly with each other [7]). Although the total density profiles also include a contribution from thermal atoms within the condensate region, we defer their analysis in this region to Sec.III B below.

Instead, we focus first here on the representation of thermally excited atoms outside the condensate region. These atoms populate the “wings” $R < |z| < z_T$, as illustrated in Fig.6(d). In this interval, the gas is still Bose degenerate with large occupation numbers per mode. Here, the data is well described by a semi-classical ideal gas model. At each phase space point (z, p) with effective single-particle energy $\varepsilon(p, z) = p^2/2m + V(z)$, assuming the Rayleigh-Jeans law (equipartition) for the

occupation numbers, gives a density

$$n_{\text{RJ}}(z) = \int_{-p_{\text{max}}}^{+p_{\text{max}}} \frac{dp}{2\pi\hbar} \frac{k_B T}{\varepsilon(p, z) - \mu} \quad (25)$$

$$= \frac{\sqrt{2}}{\pi\ell} \frac{T}{\sqrt{(V(z) - \mu)\hbar\omega}} \arctan \left[\sqrt{\frac{E_{\text{max}}}{V(z) - \mu}} \right]$$

Here, $E_{\text{max}} = p_{\text{max}}^2/2m$ is a cutoff energy that depends on the maximum kinetic energy on the grid. As shown in Fig.6(d) (dashed cyan), a good match to the sGPe data is obtained for $E_{\text{max}} = 2\pi(\ell/\Delta z)^2 \hbar\omega$ [or $p_{\text{max}} = 2\sqrt{\pi} \hbar/\Delta z$]. The divergence at $z \rightarrow \pm R$ is an artefact due to an infrared divergence of the semiclassical approximation.

Repeating this analysis with the Bose-Einstein distribution gives a density

$$n_{\text{BE}}(z) = \int \frac{dp}{2\pi\hbar} \bar{N}(\varepsilon(p, z) - \mu) \quad (26)$$

$$= \frac{1}{\ell} \sqrt{\frac{k_B T}{2\pi\hbar\omega}} g_{1/2}(x)$$

where $x = \exp[(\mu - V(z))/k_B T]$ and the Bose function has the asymptotics $g_{1/2}(x) \approx x$ for $x \ll 1$. Good agreement with the ncB data is obtained in the limit of infinite

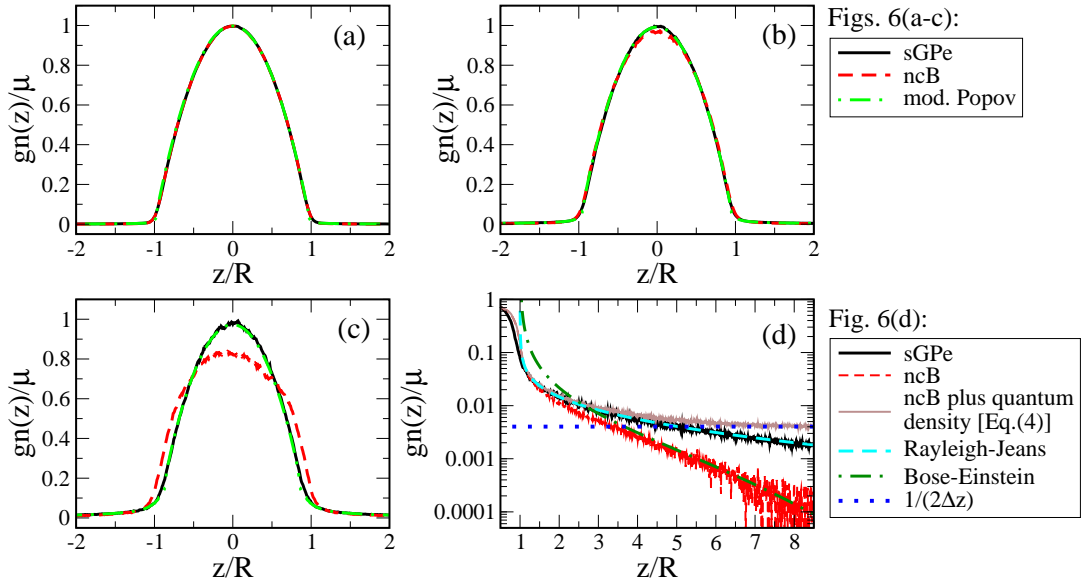


Figure 6: (Color online) Average density profiles $n(z)$, normalized as $gn(z)/\mu$, returned by the stochastic Gross-Pitaevskii equation (solid black) after an equilibration time t_{eq} and by the number conserving Bogoliubov expansion (dashed red). Plots (a)–(c) are for temperatures $k_B T = 46, 140, 430 \hbar\omega$ listed in Table II, R is the Thomas-Fermi radius at $T = 0$ [Eq.(24)]. The dot-dashed green curves give the prediction of the modified Popov theory, as developed by Andersen & al [6]. Plot (d) analyzes, on a logarithmic scale, the density in the “thermal wings” of plot (c) for $R < z \lesssim z_T$ where z_T (grey vertical line) is the point where the trap energy becomes comparable to temperature, $V(z_T) = k_B T + \mu$. The Rayleigh-Jeans density (dashed cyan) and the Bose-Einstein density (dot-dashed green) are calculated for an ideal gas. The brown solid line corresponds to the ncB density plus the quantum density level which asymptotes to the latter, n_q [Eq.(4)], indicated by the blue dotted line.

cutoff, see Fig.6(d) dot-dashed green). Indeed, it is easy to see that the contribution of momenta above p_{\max} is exponentially small provided $E_{\max} \gg k_B T$, as is the case here.

At positions beyond z_T , the gas enters a non-degenerate regime where the occupation numbers are small for a large range of momenta. Indeed, the fugacity satisfies $\exp[(\mu - V(z))/k_B T] \ll e^{-1}$ for $|z| \gg z_T$, and one can make the Boltzmann approximation, $n(z) \propto \exp[-V(z)/k_B T]$. This corresponds to the “thermal cloud” familiar from the bimodal density distributions of a partially condensed Bose gas in a trap [2]. The ncB data provides a smooth crossover into this region provided the subtraction of the quantum density is performed. The brown solid line in Fig.6(d) shows the non-subtracted density that reduces to a flat background of quantum density, $n(z) = n_q$, in the “Boltzmann tail”. In this region, the actual number of atoms per mode is much smaller than unity, and classical field methods are no longer strictly justified.

By comparing the Rayleigh-Jeans and the Bose-Einstein densities [Fig.6], it is clear that the sGPe overestimates the number of atoms in the thermal wings. The numbers that one gets by integrating $n_{RJ}(z)$ and $n_{BE}(z)$ in this region, are quite small, however, when compared to the total number of atoms. This is summarized in the last two columns of Table III. In the following, we calcu-

	$k_B T / \hbar\omega$	$\langle N \rangle [-z_T, z_T]$		$\langle N \rangle$ wing RJ – BE	$\langle N \rangle$ tail BE
		sGPe	ncB		
(a)	46	20 007	19 994	30.9	7.5
(b)	140	20 132	19 981	114.9	24.6
(c)	430	20 795	20 498	338.6	78.5

Table III: Average atom numbers in the “classical region” outside the condensate and beyond. First and second column: average number within $|z| < z_T$ where $V(z) \leq \mu + k_B T$, as obtained from the numerical simulations (including the Wigner subtraction for the tWncB data). Columns three and four are based on the ideal gas densities obtained in the classical approximation (Rayleigh-Jeans law) and using Bose-Einstein occupation numbers. The column “wing” gives the excess atoms present in the non-condensate, but still highly populated region $R \leq |z| \leq z_T$ outside the condensate (Thomas-Fermi radius R). The column “tail” gives the atoms that are located in the “tails” $z_T \leq |z| < \infty$ of an ideal gas with the Bose-Einstein distribution. For the Bose-Einstein density, an infinite momentum cutoff is taken, as in Eq.(26). For the Rayleigh-Jeans density (26), we take a kinetic energy cutoff $E_{\max} = 2\pi(\ell/\Delta z)^2 \hbar\omega$ with grid spacing Δz as given in Table II.

late the total atom number by integrating the density of each method between $z = -z_T \dots z_T$, where the classical approximation is valid.

Consider now the significant difference between sGPe and ncB in Fig.6(c), that occurs within the condensate region at the highest temperature. We attribute this to the large thermal amplitudes of the Bogoliubov modes that are no longer small compared to the condensate mode (see Fig.5), and therefore the calculation of the non-condensate density has to be done more carefully. In the modified Popov theory of Ref.[6], fluctuations are split into contributions to the density and phase, and phase fluctuations are systematically discarded when calculating the average density. We find that the sGPe data agrees well with this total density and are therefore confident that it captures the correct result.

B. Condensate and thermal excitations

Having considered the total atomic density profiles, a further important temperature-dependent quantity is the condensate fraction. The classical field methods under consideration here provide a unified description of the lowest modes of a trapped Bose gas, and so further analysis is necessary to isolate the condensate fraction, as in experiment. We choose to compare the coherent and incoherent phases of the gas, and so focus on a partitioning based on those atoms within the Penrose-Onsager ground state, and those in orthogonal states [53].

1. Density profiles and depletion

The phase coherent fraction of the gas is identified by making use of the Penrose-Onsager (PO) criterion for Bose-Einstein condensation [113]. The stochastic simulations provide us, again through the operator-classical field correspondence, with the so-called one-body-density matrix $\rho(z, z') = \langle \psi^*(z) \psi(z') \rangle$. This matrix is hermitian and positive; evaluating its trace by integrating spatially, we get $\langle N \rangle$ in the sGPe method, and $N + \mathcal{M}/2$ within the ncB approach. The PO criterion states that Bose-Einstein condensation has occurred when the largest eigenvalue of $\rho(z, z')$, denoted here by $\langle N_c \rangle$, is comparable to N , the other eigenvalues being much smaller [9]. The eigenvector ϕ_c corresponding to $\langle N_c \rangle$ gives us the (PO) ‘condensate mode’, whose spatial width characterizes the long-range phase coherence of the degenerate Bose gas. This mode provides a numerical way to implement the splitting in Eq.(5) between condensate and excitations, since we get the condensate amplitude from

$$a_c = \Delta z \sum_z \phi_c^*(z) \psi(z), \quad (27)$$

and $\psi_\perp(z) := \psi(z) - a_c \phi_c(z)$ is by construction orthogonal to ϕ_c .

Figure 7 plots the condensate density $n_c(z) = \langle N_c \rangle |\phi_c(z)|^2$ and the ‘thermal density’ $n_{th}(z) = n(z) - n_c(z)$, with corresponding thermal fractions given in Table IV. At the lowest temperature (left images), the condensate dominates [Fig.7(a)] and the thermal density is globally weak [Fig.7(d)]. The two broad peaks at $z \sim \pm R$ arise because the repulsive interaction with the condensate pushes the thermal component out of the trap center. In the intermediate temperature data (middle images), the thermal fraction is larger, yet the two methods give good agreement, with only a marginal difference in the peak value of the condensate density which now becomes noticeably smaller than the $T = 0$ solution for the same μ (thin blue line). At the relatively higher temperature $k_B T = 430 \hbar \omega$ (right images), the two methods disagree: their condensates are similar in axial extent, but the tWncB mode (dashed red) has a lower peak than the sGPe (solid black), so contains fewer atoms, and as a result the thermal fraction is higher. For all temperatures, the approximate condensate mode constructed in the ncB theory [$\phi_c(z)$ as given in Eq.(A1); dot-dashed, blue] agrees well with the PO condensate extracted from the density matrix of the ncB simulations (dashed red): we show data in Fig.7(c) only as these quantities become indistinguishable at lower temperatures.

Although the modified Popov theory inherently solves for the quasi-condensate density, $n_{qc}(z)$ (rather than the phase coherent, Penrose-Onsager condensate mode plotted here), we also show in Fig. 7(c) a prediction for the phase coherent condensate which may be extracted from the modified Popov approach (dot-dashed, green curves), and whose calculation does not require the full one-body density matrix, as we discuss in more detail in Sec.IV. At this moderate temperature, this prediction agrees well with the sGPe, except for a small region near the centre; at lower temperatures, we have found an even better agreement.

The difference between the ncB and sGPe results is likely due to the overestimation of the thermal density in the condensate region within ncB. Consider the complex values of $\psi(z)$ in the bottom images of Fig.5 for $z \lesssim R$: the density is determined by the modulus of $\psi(z)$, and the tWncB data clearly have more points with larger modulus. Another reason may be the way the Bogoliubov energy spectrum is calculated: indeed, it is based on a condensate wave function, denoted ϕ_0 in Eq.(A1), which contains all the particles of the system, whereas an improved approach would account for the depletion of the condensate in calculating the Bogoliubov spectrum. To illustrate this, we consider as a first step an improved spectrum based upon a condensate with the same number of atoms as contained within the sGPe PO condensate. The thermal density which results is shown as the dotted maroon line in Fig. 7(f), and is al-

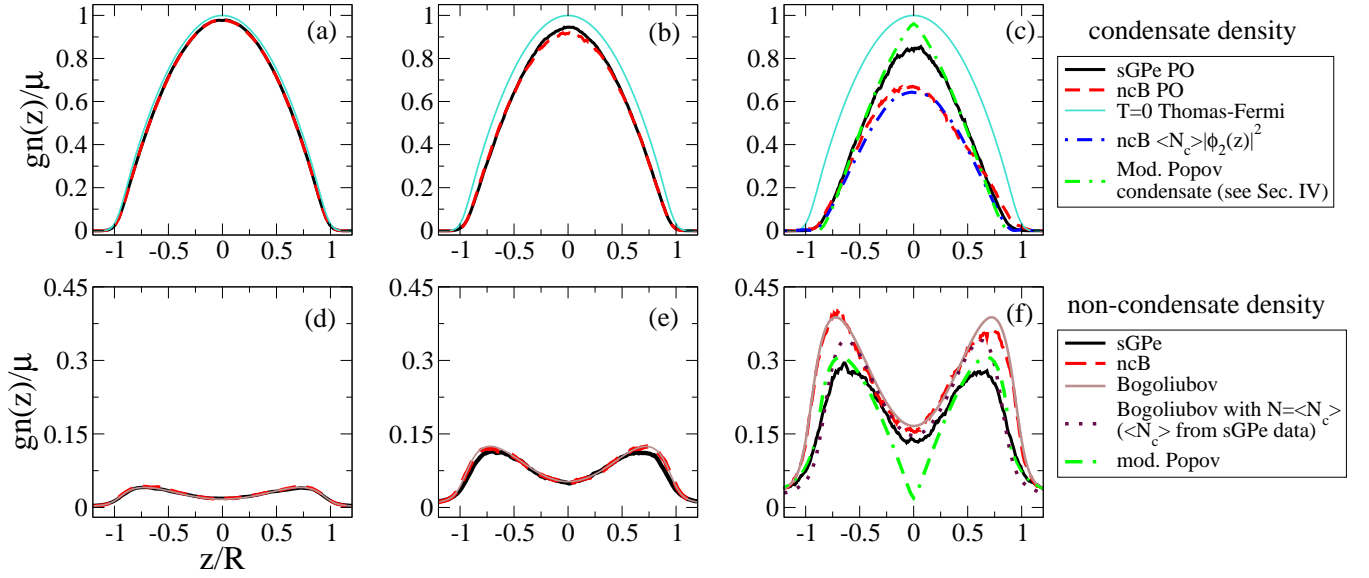


Figure 7: (Color online) Condensate (top row) and thermal cloud (bottom row) densities for temperatures (a),(d) $k_B T = 46 \hbar\omega$; (b),(e) $k_B T = 140 \hbar\omega$; and (c),(f) $k_B T = 430 \hbar\omega$. Condensate density $n_c(z) = \langle N_c \rangle |\phi_c(z)|^2$ obtained from Penrose-Onsager analysis of the one-body density matrix [sGPe: solid, black; tWncB: dashed, red]. Also shown for reference is the $T = 0$ stationary solution to the GP equation with eigenvalue μ (thin solid, turquoise), which coincides with the zeroth order condensate mode within ncB. In (c) the condensate density $\langle N_c \rangle |\phi_2(z)|^2$ following the 2nd order correction within the ncB expansion is also shown (dot-dashed, blue), as well as the modified Popov condensate density (dot-double dashed, green) [see Sec.IV Eq.(56) for details]. Bottom row: thermal density $n_{th}(z) = n(z) - n_c(z)$ [sGPe: solid black; tWncB: dashed red]. As in Fig.6, the Wigner correction was made for the tWncB case. Shown in (d–f) is the $T = 0$ Bogoliubov prediction, Eq.(A4), with N (solid brown) and, in (f) only, also $N = N_{PO}$ of the sGPe (dotted maroon), alongside the modified Popov result (dot-double dashed, green).

	$k_B T / \hbar\omega$	sGPe	tWncB
(a)	46	0.0474	0.0468
(b)	140	0.141	0.143
(c)	430	0.365	0.450

Table IV: Thermal fraction $\langle N_{th} \rangle / \langle N \rangle$ versus temperature for the sGPe and tWncB initial states for the three chosen temperatures, where $\langle N_{th} \rangle$ is the integral over $n_{th}(z)$ in the region $|z| < z_T$, and the correction due to symmetric operator ordering is applied to the tWncB data as for Fig.6.

ready in better agreement with both the sGPe and modified Popov results, despite the quite rudimentary nature of the modification to the Bogoliubov spectrum.

The thermal fraction, $\langle N_{th} \rangle / \langle N \rangle = 1 - \langle N_c \rangle / \langle N \rangle$, varies slightly depending on the simulation method, as shown in Table IV. Since the total atom number N varies across the statistical ensembles, we calculate the condensate fraction from $\langle N_c \rangle / \langle N \rangle$. We observe again larger values for this quantity in the tWncB method at higher temperatures (row (c)). We suggest that the depletion in this range is not small enough to warrant the ncB expansion around a “large” condensate. Indeed, if we identify from Eq.(14), Ref.[80], $(N_{th}/N_c)^{1/2}$ as a small expansion parameter, within the ncB calculation this reaches the

value ≈ 0.90 that is clearly not small.

2. Condensate shape

The back action of the non-condensate particles can be made visible by a careful analysis of the shape of the condensate wave function $\phi_c(z)$, the results of which are summarized in Fig.8. The simplest generalization of the GPe that applies to nonzero temperature is a Hartree-Fock (HF) potential due to non-condensate particles (analogous to Eq.(21))

$$\text{HF: } (H_{GP}[N_c|\phi_c|^2] + 2gn_{th}(z))\phi_c = \mu\phi_c(z) \quad (28)$$

where the thermal density is

$$n_{th}(z) = \langle \hat{\psi}_\perp^\dagger(z) \hat{\psi}_\perp(z) \rangle \quad (29)$$

One could however also take into account the anomalous average $m(z)$ due to non-condensate modes. If the condensate field $a_c\phi_c$ is chosen real, the anomalous average is simply given by

$$m(z) = \langle \hat{\psi}_\perp(z) \hat{\psi}_\perp(z) \rangle. \quad (30)$$

(A definition not based on U(1) symmetry breaking can be found in Eq.(47) below.) Within the Bogoliubov ap-

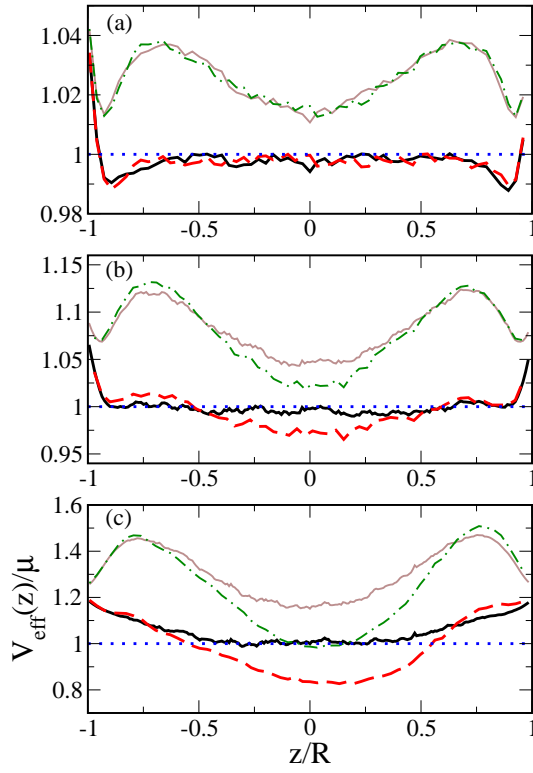


Figure 8: (Color online) Analysis of the back-action of the non-condensate atoms on the shape of the condensate mode ϕ_c . We plot the effective potential of Eq.(34) with (lower curves, HFB theory) and without the last term (upper curves, HF theory), normalized to μ . The condensate mode function $\phi_c(z)$ is taken from a Penrose-Onsager analysis of the one-body density matrix. Solid black/brown lines: sGPe data, (dot-)dashed red/green lines: tWncB data. The HFB theory that includes the back action from the anomalous average is closer to the actual chemical potential.

proximation, one has

$$n_{\text{th}}(z) = \sum_k \{ \bar{N}(E_k) |u_k(z)|^2 + (\bar{N}(E_k) + 1) |v_k(z)|^2 \}, \quad (31)$$

$$m(z) = \sum_k (2\bar{N}(E_k) + 1) u_k(z) v_k^*(z). \quad (32)$$

(In a homogeneous gas of dimensions $D \geq 2$, the sums in Eqs.(31, 32) are ultraviolet divergent [10, 11, 85] and are regularized routinely by a renormalized coupling constant. This is not needed in the one-dimensional case considered here, due to the decay of $v_k(x)$ for $E_k \gg \mu$.) This leads to the following ‘Hartree-Fock-Bogoliubov (HFB) extension of Eq.(28):

$$\text{HFB: } (H_{\text{GP}}[N_c |\phi_c|^2] + 2gn_{\text{th}}(z)) \phi_c + gm(z) \phi_c^* = \mu \phi_c(z) \quad (33)$$

where we allowed momentarily for a complex-valued condensate wave function to illustrate the $U(1)$ invariance of the theory [137].

The data shown in Fig.8, taken from both stochastic methods, suggests that Eq.(33) is more appropriate for the (PO) condensate mode, at least in the central region of the trap. This effect, along with the role of higher anomalous averages, has been studied in detail in the context of the microcanonical pGPe theory in [114]. There are significant differences at higher temperatures in the tWncB data, similar to those appearing in the average density. We recall that the HFB theory has been put into question because it leads, for a homogeneous system, to a gapped excitation spectrum, in contradiction to the Hugenholtz-Pines theorem [30–34, 52].

One should also compare to the modified Popov theory (Sec.II E). Indeed, we can interpret the HFB potential in Eq.(33) for the condensate mode, as a modification of the thermal density. Going back to a real-valued condensate $\phi_c(z)$, the effective potential in Eq.(33) takes the form

$$V_{\text{HFB}} = V + gN_c \phi_c^2 + 2gn_{\text{th}} + gm \quad (34)$$

while the last term is missing in Eq.(28). Now in Bogoliubov theory, we have (adopting real mode functions normalized according to Eq.(A6))

$$\begin{aligned} n_{\text{th}}(z) + m(z) &= \sum_k \{ \bar{N}_k (u_k(z))^2 + (\bar{N}_k + 1) (v_k(z))^2 \\ &\quad + (2\bar{N}_k + 1) u_k(z) v_k(z) \} \\ &= \sum_k \{ \bar{N}_k (u_k(z) + v_k(z))^2 + (u_k(z) + v_k(z)) v_k(z) \} \end{aligned} \quad (35)$$

with the shorthand $\bar{N}_k = \bar{N}(E_k)$. Equation (35) is closely related to the thermal density n'_{th} of the modified Popov theory [Eq.(19)] which can be expressed in terms of Bogoliubov amplitudes (normalized to $u_p^2 - v_p^2 = 1$) as

$$\begin{aligned} n'_{\text{th}} = n - n_{\text{qc}} &= \frac{1}{V} \sum_p \{ \bar{N}_p (u_p + v_p)^2 \\ &\quad + (u_p + v_p) v_p + \frac{gn_{\text{qc}}}{2\epsilon_p + 2\mu} \} \end{aligned} \quad (36)$$

This clearly contains an additional term; this term is, however, small in the temperature regime considered for our numerical simulations, leading to a good analogy when the above re-interpretation of mean field potentials is made. This is in fact somewhat analogous to the work of Ref.[115].

The analogy cannot be pushed further, since the modified Popov theory does not directly deal with the condensate mode (in the PO sense), but with the quasi-condensate. See Sec.IV for a link between the two quantities.

C. Correlation functions

The focus in this section is upon spatial coherence in phase and density. These show a rich physics in weakly

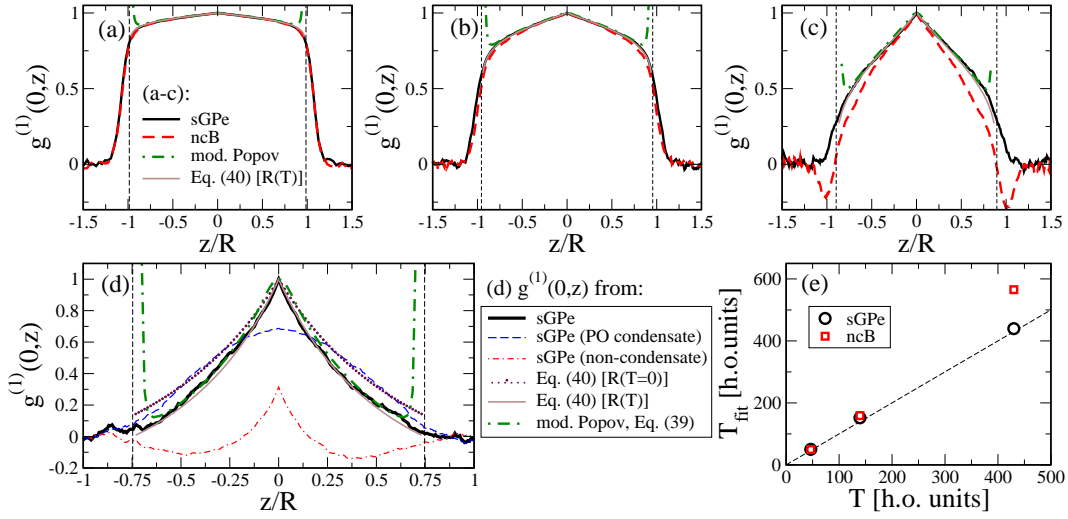


Figure 9: (Color online) First order correlation function $g^{(1)}(z) = g^{(1)}(0, z)$, as defined in Eq.(37), from the sGPe data (solid black) and the ncB data (dashed red). Temperatures in (a–c) as given in Table II, in (d), we have $T \approx 1.3 T_\phi$ (only sGPe data shown). We plot the real part of $g^{(1)}(z)$, the imaginary part being negligibly small. Dot-dashed green lines: Eq.(39), based on modified Popov theory. Brown, dotted lines: Eq.(40), In (d), we plot Eq.(40) using $R(T) < R$ (solid thin brown) and $R(T) = R$ (dotted orange). The contributions from the sGPe Penrose-Onsager condensate mode (dashed blue) and from non-condensate modes (dot-dashed red) are shown separately, from Eq.(43). In (a–d) the vertical dashed thin lines indicate $R(T)$. (e) Estimated temperature based on fitting $g^{(1)}(z)$ near $z = 0$ to Eq.(42) (dashed line) for sGPe (black circles) and ncB (red squares).

interacting one-dimensional Bose systems due to the separate characteristic temperatures for the suppression of phase and density fluctuations.

1. First-order coherence: phase fluctuations.

To study the phase coherence, we begin with the first-order coherence function (a normalized one-body density matrix)

$$g^{(1)}(z', z) = \frac{\langle \psi^*(z') \psi(z) \rangle}{[n(z)n(z')]^{1/2}} \quad (37)$$

where $n(z)$ is the average density and the normalization gives $g^{(1)}(z, z) = 1$. For simplicity, we fix one position in the trap centre, $z' = 0$, and write $g^{(1)}(z) = g^{(1)}(0, z)$. As illustrated in Fig.9, $g^{(1)}(z)$ scales roughly linearly in the centre and drops quickly to zero towards the border of the condensate mode ($z \sim R$). The slope in the centre agrees well between the two methods (sGPe vs. ncB: solid black vs. dashed red), but for $z \sim R/2$, differences appear at the highest temperature. Quite striking are the negative values for $g^{(1)}(z)$ which then occur, within the ncB formalism, in the region of the Thomas-Fermi radius (anti-correlation between central region and condensate edge).

At the low temperatures probed, the behaviour of $g^{(1)}(z)$ compares well with the theory of phase fluctuations in weakly interacting Bose gases: One starts from

the *Ansatz*

$$g^{(1)}(z) = \exp[-\langle (\hat{\theta}(z) - \hat{\theta}(0))^2 \rangle / 2] \quad (38)$$

and works out the thermal statistics for the phase operator $\hat{\theta}(z)$.

From this point, the required exponent may be calculated within the modified Popov theory [7, 112, 116]. Making the classical approximation $\bar{N}(E_j) \approx k_B T / E_j$, we can write this exponent as

$$\begin{aligned} & \langle [\hat{\theta}(z) - \hat{\theta}(0)]^2 \rangle \\ &= \frac{4T}{3T_\phi} \sum_{j>0} \left[\frac{2j+1}{j(j+1)} (P_j(z/R(T)) - P_j(0))^2 \right. \\ & \quad \left. - \frac{(2j+1)(\hbar\omega)^2}{8\mu^2} \left(\frac{P_j(z/R(T))}{1 - z^2/R(T)^2} - P_j(0) \right)^2 \right]. \end{aligned} \quad (39)$$

where $P_j(z)$ are Legendre polynomials of order j . Here $k_B T_\phi \approx 40 \mu$ is the characteristic temperature for phase fluctuations [Eq.(1)].

The first term of Eq.(39) was derived by Petrov *et al.* [4] who, focussing on the temperature range $\hbar\omega \ll k_B T$, did not explicitly include in their expression the temperature dependence of the Thomas-Fermi radius $R(T)$. For the parameters considered, the second term within the sum of Eq.(39) typically gives a small contribution, but leads to a rounding off of the central peak in $g^{(1)}(0, z)$. This additional term leads to a divergence in $g^{(1)}(0, z)$, however, as $|z| \rightarrow R(T)$, due to the assumption that the condensate density is parabolic. The results

of Eq.(39) are shown by the dot-dashed, green curves in Fig. 9. In particular, at the highest temperature (panel (d)), the shrinking of the quasi-condensate ($R(T) < R$) is clearly seen, due to the increased thermal component of the density.

A closed form for $g^{(1)}(0, z)$ may be obtained by neglecting the second term of Eq.(39), since the mode summation for the first term can be performed analytically, as pointed out previously in [4, 117]. This gives

$$\langle [\hat{\theta}(z) - \hat{\theta}(0)]^2 \rangle = \frac{4T}{3T_\phi} \left| \log \left(\frac{1 + z/R(T)}{1 - z/R(T)} \right) \right|, \quad (40)$$

where we have kept the temperature-dependent Thomas-Fermi radius, thereby generalizing the expressions of Refs.[4, 117]. We note that Ghosh considered a quantized hydrodynamic approach to the correlations of a quasi-1d Bose gas [118], which also extends the work of Petrov *et al.* in Ref. [4]. Eq.(40) is shown with $R(T)$ taken from the modified Popov simulations by the solid, thin brown lines in Figs. 9(a–d) and agrees well with the numerical data. At the highest temperature [Fig. 9(d)], we see a clear deviation between an approach like the modified Popov theory that takes condensate depletion into account (taking $R(T) < R$, solid, thin brown), and the original expression of Ref.[4] where the condensate size is fixed at a constant Thomas-Fermi radius (dotted orange).

In the central trap region $|z| \ll R$, we can approximate Eq.(40) as

$$\langle (\theta(z) - \theta(0))^2 \rangle \approx \frac{2z}{L_\phi(T)}, \quad L_\phi(T) = \frac{3T_\phi}{4T} R(T), \quad (41)$$

where $L_\phi(T)$ is the phase correlation length. This expression illustrates that as $T \geq T_\phi$, the system is (first-order) coherent over a scale significantly shorter than the Thomas-Fermi radius [4]. Assuming $R(T) \approx R$ and using the Thomas-Fermi formula for the condensate profile, we can re-write the product $T_\phi R$ in Eq.(41) in a model-independent way

$$|z| \ll R: \quad g^{(1)}(z) \approx 1 - \frac{g}{2\hbar\omega\ell} \frac{z k_B T}{\ell \mu}. \quad (42)$$

Based upon Eq.(42), the slope of $g^{(1)}(z)$ in the region $0 < z \lesssim R/2$ yields an independent measure of the temperature. We compare the temperature extracted in this way (denoted T_{fit}) to the input temperature of the simulations. Both simulations give coherence functions $g^{(1)}(z)$ that are consistent with Eq.(42), except for the ncB data at $T \approx 0.25 T_\phi$ where the phase coherence is decaying faster. The ensemble prepared by ncB in the latter case appears not only to be at a higher temperature (as in Fig.7(c)), it is actually not even stationary, as we illustrate in Sec.V. Let us come back to the link between the phase coherence function $g^{(1)}$ and the one-body density

matrix. As explained in Sec.III B, the latter can be expanded in orthogonal modes, with the (PO) condensate mode $\phi_c(z)$ giving the dominant contribution. In the notation of the ncB approach [Eq.(5)], one can decompose the stochastic wavefunction in condensate and excitation parts, $a_c \phi_c(z) + \psi_\perp(z)$, where $\psi_\perp(z)$ represents all modes orthogonal to the PO mode. The first order correlation function may then be broken down into

$$\langle \psi^*(0) \psi(z) \rangle = \langle N_c \rangle \phi_c^*(0) \phi_c(z) + \langle \psi_\perp^*(0) \psi_\perp(z) \rangle. \quad (43)$$

This gives two contributions to $g^{(1)}(z)$ that are illustrated in Fig.9(d). The condensate mode (dashed blue) provides the largest contribution and is positively correlated. The contribution due to modes orthogonal to the PO mode (dot-dashed red) becomes negative towards the condensate border because these modes have additional nodes (only even mode functions contribute). This reduces $g^{(1)}(z)$ below the condensate contribution. The “spike” near the centre is also due to higher modes and contains the approximately exponential decay due to phase fluctuations [Eqs.(38, 41)] that becomes narrower as $T \sim T_\phi$.

2. Second-order coherence: density fluctuations

We now consider correlations of order four, namely fluctuations of the atomic density. These are captured by the coherence function

$$g^{(2)}(z) = \frac{\langle |\psi(z)|^4 \rangle}{[n(z)]^2}. \quad (44)$$

In terms of field operators, we actually consider the probability of detecting two atoms at z , $g^{(2)}(z) \propto \langle \hat{\Psi}^\dagger \hat{\Psi}^\dagger \hat{\Psi} \hat{\Psi} \rangle$. This operator ordering is mapped to the following combination of tW data:

$$\langle \hat{\Psi}^\dagger \hat{\Psi}^\dagger \hat{\Psi} \hat{\Psi} \rangle = \langle |\psi(z)|^4 \rangle_W - 4 \langle |\psi(z)|^2 \rangle_W n_q + 2n_q^2 \quad (45)$$

where n_q is the quantum density level on the grid [Eq.(4)]. The local density $n(z)$ used for normalization is also Wigner-corrected and given by Eq. (A12). The sGPe data are taken as in Eq. (44).

It is well known that for a single-mode coherent field, $g^{(2)}(z) = 1$, while for a chaotic (multi-mode) field with Gaussian statistics, $g^{(2)}(z) = 2$ [119, 120]. Antibunching, $g^{(2)}(z) < 1$, is a non-classical effect that we do not expect within the classical stochastic theories used here; it occurs indeed at lower temperatures, see Refs.[75, 121]. Any value in between the limits 1 and 2 is thus a measure of how many modes effectively contribute to the density. The data shown in Fig.10 follows the expected behaviour [44, 116, 120, 122]: a flat plateau in the center and a jump from 1 to 2 at the border of the condensate. (The oscillations outside the center are

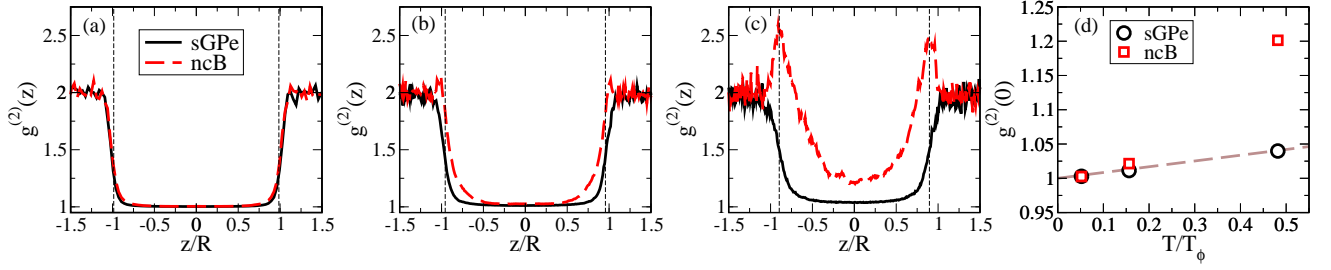


Figure 10: (Color online) Density correlation function $g^{(2)}(z)$ [Eq.(44)] from the sGPe simulations (solid black) and the ncB simulations (dashed red). For the ncB case, the corrections of Eq.(45) are applied, so that in the quantum field theory, $g^{(2)}(z)$ has the meaning of a second-order coherence function. The vertical dashed thin lines indicate $R(T)$ at the temperatures in (a–c), which are as in Table II. (d) Comparison of results for $g^{(2)}(0)$ (black circles: sGPe, red squares: tWncB) with Lieb-Liniger theory, Eq.(46), taken from Ref.[75] (dashed brown).

statistical errors that are enhanced by the normalization in Eq.(44).) The jump at the Thomas-Fermi radius becomes more gradual as the temperature rises, and the single-mode region shrinks [116]. At the highest temperature, the ncB theory gives anomalously large values $g^{(2)}(z) > 2$ near the condensate border.

Since the lowest excitation modes of the condensate carry mainly phase fluctuations [2], we expect a significant deviation from $g^{(2)}(z) = 1$ to set in at a higher temperature compared to $g^{(1)}(z)$. This can be made more precise by comparing to Ref.[75] where Kheruntsyan *et al.* use exact solutions of the Lieb-Liniger model, within the local-density approximation, to calculate the density correlation in a trapped gas. Their result for the trap center, within the weakly interacting regime $\mu \ll 2k_B T \ll k_B T_d = N \hbar \omega$ of interest here, is (Eq. (5.10) of [75]):

$$g^{(2)}(0) \approx 1 + \frac{4\sqrt{2} T}{3T_d}. \quad (46)$$

The linear increase in temperature is in good agreement with the results of our classical field simulations, see Figure 10(d), and [116]. The high-temperature ncB data, however, is much too large compared to both the sGPe and Lieb-Liniger theory. This suggests either a higher temperature, consistent with the findings of previous tests, or a significant overestimation of density fluctuations. We mention that values $g^{(2)}(z) \rightarrow 3$ [123] would arise when the field $\psi(z)$ has a fixed phase and behaves like a real-valued random number. This is related to a large contribution from the ‘squeezing correlation’ $m(z) \sim \langle \psi(z)\psi(z) \rangle$ that we discuss now.

3. Squeezing and anomalous average

We finally consider the anomalous average of the non-condensate field defined as (cf. [124])

$$m(z) = \left\langle \frac{[(a_c \phi_c(z))^* \psi_\perp(z)]^2}{|a_c \phi_c(z)|^2} \right\rangle \quad (47)$$

where $a_c \phi_c(z)$ is the component of the matter wave field along the condensate mode [Eq.(27)] and $\psi_\perp(z)$ is the perpendicular component. Note that $m(z)$ as defined in Eq.(47) is invariant under global phase transformations of both the total field $\psi(z)$ and the condensate mode function $\phi_c(z)$. It vanishes if the condensate amplitude a_c and $\psi_\perp(z)$ have no fixed phase relation: we thus probe the phase locking between the condensate and non-condensate fields. We use for our data analysis the Penrose-Onsager condensate mode introduced in Sec.III B. This interpretation of the anomalous average can be re-phrased in the squeezing language of quantum optics [125]: the interference term between condensate and non-condensate fields is split in two quadrature fields (both have the dimension of a density)

$$(a_c \phi_c(z))^* \psi_\perp(z) = X_n(z) + iX_\theta(z). \quad (48)$$

The real part X_n indeed gives the (local) density fluctuation on top of the condensate density $|a_c \phi_c(z)|^2$, while the imaginary part X_θ describes phase fluctuations (if these are small). On average, these quadratures are zero, and the difference of their variances is

$$\langle X_n^2(z) \rangle - \langle X_\theta^2(z) \rangle = \text{Re} \langle [(a_c \phi_c(z))^* \psi_\perp(z)]^2 \rangle \quad (49)$$

which is just the real part of $m(z)$ defined in Eq.(47). The sum of these variances equals the normalization factor in Eq.(47) times the non-condensate density $n_{\text{th}}(z) = \langle |\psi_\perp(z)|^2 \rangle$.

Within the Bogoliubov approximation, we calculate $m(z)$ by choosing a phase reference where the condensate field $\phi_c(z)$ is real-valued. By expanding $\psi_\perp(z)$ over Bogoliubov modes with operator amplitudes $\beta_k = a_c^* b_k / |a_c|$ instead of b_k , global phase invariance holds (see Refs.[70, 80, 137]). In the Bogoliubov limit, condensate number fluctuations can be ignored, $|a_c|^2 = \langle N_c \rangle$,

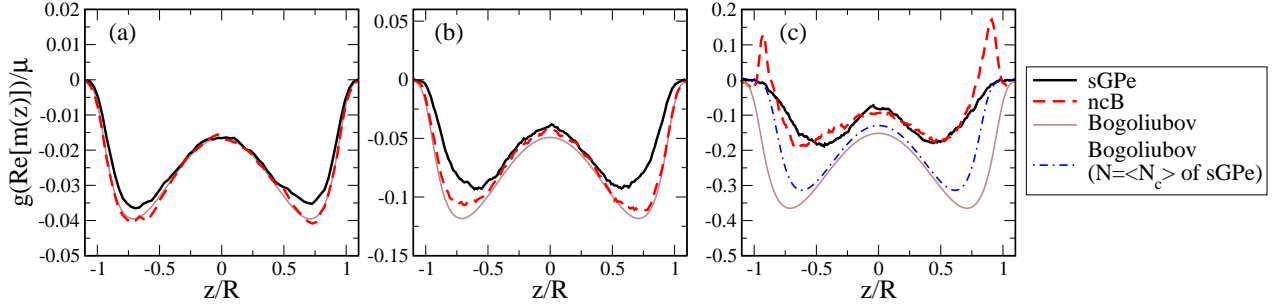


Figure 11: (Color online) Real part of the squeezing correlation (anomalous average) $m(z)$, as defined in Eq.(47), for the temperatures of Table II. Solid black: sGPe result, dashed red: ncB result. The Bogoliubov result (solid brown, Eq.(32)) is calculated with the mode functions of the $T = 0$ BdG operator (A3), and also using the Bogoliubov spectrum calculated for a condensate number equal to the sGPe PO condensate number (blue, dot-dashed).

and we recover Eq.(32)

$$\begin{aligned} m(z) &= \sum_k \langle (u_k(z)\beta_k + v_k^*(z)\beta_k^\dagger)(u_k(z)\beta_k + v_k^*(z)\beta_k^\dagger) \rangle \\ &= \sum_k (2\bar{N}(E_k) + 1) u_k(z)v_k^*(z) \end{aligned} \quad (50)$$

where $\bar{N}(E_k) = \langle \beta_k^\dagger \beta_k \rangle$. This quantity is thus sensitive to the ‘anomalous’ or ‘hole’ part $v_k(z)$ of the Bogoliubov modes. In particular, we note that the anomalous average shows a quite precise linear scaling in T in the temperature range of interest. This illustrates the relative dominance of highly populated modes that are well described within the classical approximation.

The data in Fig.11 show a reasonable qualitative agreement between the stochastic simulations and Bogoliubov theory: $m(z)$ has a large negative real part. Beyond this, there are clearly differences on a quantitative level, particularly as temperature is increased. Note that the anomalous average is of comparable magnitude to the non-condensate density $n_{\text{th}}(z)$, which points towards a strong enhancement of the phase fluctuation quadrature $X_\theta(z)$ relative to density fluctuations. The agreement between sGPe (solid black) and ncB (dashed red) remains reasonable at all temperatures considered in our comparison, however both theories deviate from the ($T = 0$) Bogoliubov prediction (brown, solid line). Also shown in Fig. 11 is the result of Eq.(50), calculated with Bogoliubov mode functions for a condensate with a reduced number of atoms: we have replaced in the Bogoliubov–de Gennes operator $N|\phi_0|^2$ by $\langle N_c \rangle |\phi_c|^2$, where $\langle N_c \rangle$ is obtained from the sGPe. Note that this does not significantly improve the agreement, unlike the case of the thermal density of Fig.7(f). The enhancement of phase fluctuations is nicely illustrated in Fig.12 where the realizations of the complex field $\psi(z)a_c^*/|a_c|$ are plotted. The additional phase factor, relative to the data of Fig.5, removes the random phase of the condensate mode, and reveals the squeezed distribution of the complex field, with enhanced fluctuations in the quadrature

orthogonal to the condensate mode. At higher temperatures, the sGPe data show that these fluctuations are channeled into a “crescent”-shaped region, maintaining the relative suppression of density fluctuations. The ncB expansion does not take this into account, and the fluctuations keep their alignment to orthogonal quadratures so that density fluctuations (in the radial direction) become too large. This clearly happens when the phase difference across different points in the system becomes comparable (in standard deviation) to $\pi/2$ so that linearization procedures break down (“quasi-condensate regime”).

D. Condensate statistics and fragmentation

We analyze in this section the one-body density matrix $\langle \psi^*(z)\psi(z') \rangle$ in more detail. Its eigenvector with the largest eigenvalue corresponds to the condensate mode $\phi_c(x)$ in the sense of Penrose and Onsager, as explained in Sec.III B. The distribution function of the corresponding complex amplitude a_c [Eq.(27)] provides us with the probability of finding $N_c = |a_c|^2$ atoms in the condensate, the so-called “counting statistics”. We emphasize that this quantity depends on moments (correlation functions) of arbitrarily high order of the stochastic field. We also discuss the relative importance of non-condensate modes whose occupation grows as the temperature increases, illustrating a phenomenon similar to fragmentation [9] for $T \sim T_\phi$ and above.

1. Counting statistics

The statistics $P(N_c)$ of the number of condensate atoms has been well studied in the context of laser theory [74], and Bose-Einstein condensation [71–73, 83, 84, 98, 126, 127]. It is worth mentioning that number distributions for an ideal Bose gas provide an example where the canonical and grand-canonical ensembles of

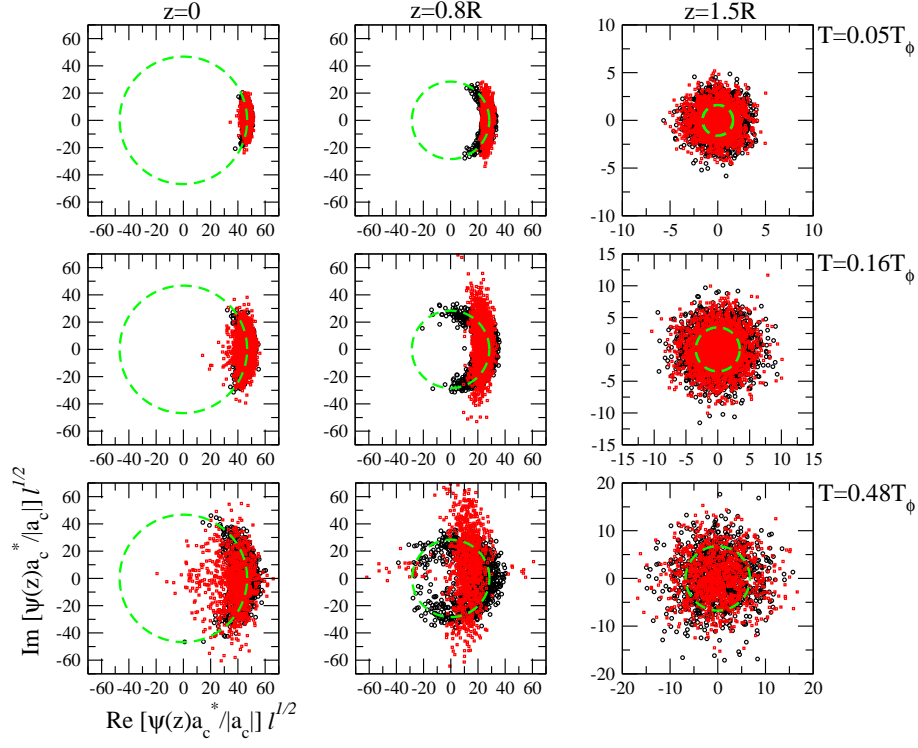


Figure 12: (Color online) Representation of the ensemble of stochastic fields $\psi(z)$, locked to the phase of the condensate mode (we multiply with $a_c^*/|a_c|$ where a_c is the amplitude (27) of the (Penrose-Onsager) condensate mode). Black: sGPe simulation, red: ncB simulation. Trap position and temperatures as in Fig.5. Note the elliptical shape of the point cloud, illustrating the relative enhancement of phase fluctuations (imaginary part). The sGPe data deform into a “crescent” shaped cloud at intermediate and high temperatures, while the ncB distribution remains aligned to orthogonal quadratures. The dashed green circles represent the Thomas-Fermi ($|z| < R$) and Bose-Einstein ($z = 1.5 R$) predictions for the square root of the density at each trap position and temperature, as in Fig.5.

thermodynamics are not equivalent: only the average atom numbers coincide, while all higher moments of the (total) atom number are anomalously large in the grand-canonical ensemble [70, 84]. This anomaly is removed in an interacting gas due to the energetic cost of adding particles to the condensate. The counting statistics $P(N_c)$ is found from the stochastic data by drafting a histogram of the values for $N_c = |a_c|^2$ across the ensemble of realizations, with a_c calculated from Eq.(27). Obviously, the N_c need not be integers here, due to the replacement of operators with classical fields. Figure 13 compares these data with the theory of Scully and co-workers (S&Co), in particular Ref.[71]. This is developed within the canonical ensemble, and treats the non-condensate modes either within Bogoliubov theory (low temperatures), or extrapolated to higher temperature with the help of a rate equation approach. We outline the main steps in Appendix B.

Reasonable agreement between the stochastic simulation methods and S&Co (dot-dashed green) is apparent at all three temperatures shown in Fig.13. At the lowest temperature [Fig.13(a)], the sGPe approach (solid black) gives a slightly a broader distribution. This broaden-

ing becomes more pronounced if the atom number is lowered [panel (d)], bringing the system closer to an ideal gas. At the highest temperature considered, the ncB distribution (dashed red) gives too much weight on small condensate numbers. This failure is particularly striking, given that the method of S&Co uses a Bogoliubov description of the non-condensate particles that is fairly close to the ncB expansion. There is one additional ingredient, however, namely the growth and depletion rates in the rate equation *Ansatz* for the counting statistics (see App. B for details): these rates are calculated as a function of N_c , while in the ncB expansion, the Bogoliubov spectrum is calculated only for the extreme case $N_c = N$. We thus expect that some effects of a strongly depleted condensate are not captured. This illustrates again the importance of self-consistently adjusting N_c within the theory as temperature is varied, see also Ref.[72].

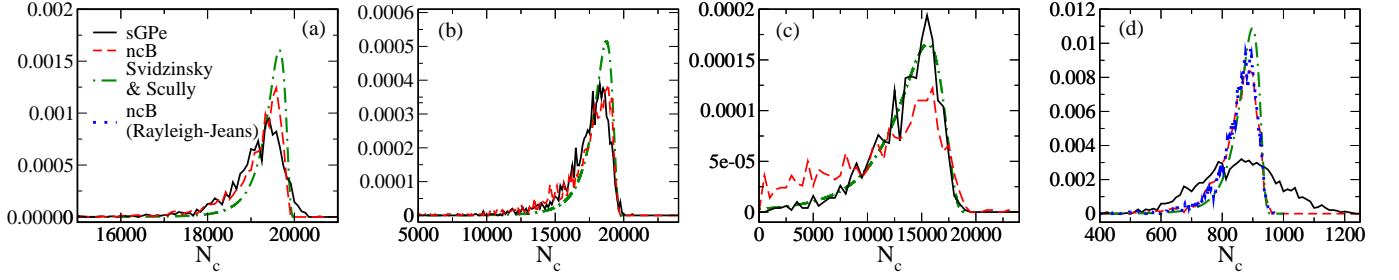


Figure 13: (Color online) Counting statistics $P(N_c)$ for the condensate number, with $N_c = |a_c|^2$, and the condensate mode in Eq.(27) obtained from the Penrose-Onsager criterion. Solid black: sGPe, dashed red: ncB, dot-dashed green: theory of Ref.[71]. Temperatures in (a–c) increase from left to right, (as in Table II), ($N \approx 20\,000$, $\mu = 22.41 \hbar\omega$). Panel (d) has $N \approx 1\,000$ ($\mu = 3.11 \hbar\omega$) and a temperature $T \approx 0.23 T_c$, the same ratio as in (c). Dotted blue line: ncB with Rayleigh-Jeans instead of Bose-Einstein occupation numbers, i.e., in Eq.(7), $\sigma_k^2 \mapsto k_B T / E_k$.

2. Discussion

It may come as a surprise that a grand-canonical approach like the sGPe where the total atom number is not fixed (i.e., values $N_c > \langle N \rangle$ are not excluded), is able to reproduce the counting statistics of number-conserving theories (like the ncB and S&Co). We attribute this to the interatomic interactions in the system that translate fluctuations in the condensate number into energetic changes. This makes the system “stiffer” and suppresses number fluctuations relative to the ideal Bose gas [70, 84]. A complementary explanation is based on the observation that the condensate mode $a_c \phi_c$ is a low-

energy subsystem of the total field (represented by ψ), where the non-condensate fraction can play the role of a particle reservoir. This suggests that the condensate subsystem can be described within a grand-canonical scheme even if the total atom number is fixed: for that it would be sufficient to consider a high enough temperature so that a large number of non-condensate atoms is present. Indeed, the width $\sigma(N_c)$ of the canonical counting statistics translates two physically different mechanisms: on the one hand, the statistical uncertainty of the non-condensate (Bogoliubov) occupation numbers in the ncB expansion (exponentially distributed with mean $\bar{N}(E_k)$), and on the other hand, the dynamical particle exchange with the non-condensate modes due to interactions, similar to what is done between system and bath within the sGPe.

These considerations also suggest an explanation for the broader statistics that the sGPe method returns at low temperatures and small numbers [Fig.13(d)]. It is symptomatic of the grand canonical ensemble which underlies the formulation of the sGPe, and leads to anomalously large number fluctuations for this nearly ideal gas. We have checked that the classical approximation underlying the sGPe is not in error here: indeed, the counting statistics of the ncB method (canonical ensemble) is essentially the same when Bose-Einstein occupation numbers are replaced by their classical (Rayleigh-Jeans) limit [Fig.13(d), dotted blue curve].

Figure 14 shows the moments of the sGPe counting statistics as a function of the total particle number. This is compared to the theory of S&Co (canonical ensemble). We vary $\langle N \rangle$ over more than one order of magnitude, as a way to change the importance of particle interactions. The temperature is kept at a fixed ratio $T/T_c = 0.23$, where $T_c = T_c(N)$ is the critical temperature for an ideal gas (see Eq.(1) and Fig. 4). The mean values [Fig.14(a)] agree well between the ensembles, as expected [70], except perhaps at the smallest particle numbers. The standard deviation [Fig.14(b)] is larger at

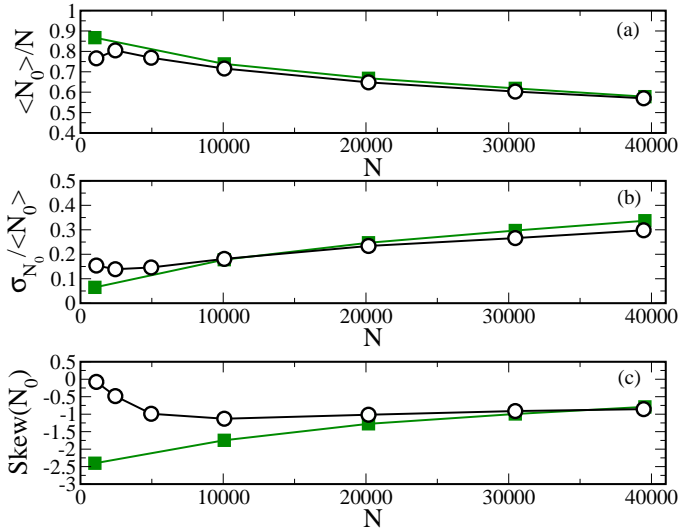


Figure 14: (Color online) First three moments of $P(N_c)$ vs. total particle number $\langle N \rangle$ of sGPe (open circles) vs. theory of Ref.[71] (filled green squares): (a) mean value $\langle N_c \rangle$ scaled to $\langle N \rangle$ (condensate fraction), (b) relative standard deviation $\sigma(N_c)/\langle N_c \rangle$, (c) skewness or third centered moment, $\text{skew}(N_c) = \langle (N_c - \langle N_c \rangle)^3 \rangle / \sigma^3(N_c)$. The total particle number N is calculated over the region $|z| < 2R$.

small $\langle N \rangle$ where one is closer to the ideal gas, but converges to S&Co theory for larger systems. In the third moment [Fig.14(c)], which measures the deviation from Gaussian statistics, we see that, at rather small numbers, the sGPe predicts a more symmetric distribution compared to the negatively skewed distribution obtained in the canonical ensemble. This suggests that in weakly interacting systems, the small non-condensate fraction cannot protect the condensate, like a “buffer”, against the Gaussian noise in the stochastic dynamics. The skewness builds up at higher particle numbers where also more modes are highly occupied, which is of course the regime where the sGPe should perform well.

3. Fragmentation

For $T \ll T_\phi$, one mode dominates the system, as many atoms are condensed and phase coherent (nearly pure condensate), whereas at higher temperatures, many modes become appreciably occupied (quasi-condensate). This behaviour can be made quantitative by considering the set of eigenvalues of the one-body density matrix $\langle \psi^*(z)\psi(z') \rangle$, i.e., the average occupations N_k of the corresponding modes ($k = 1, \dots, \mathcal{M}$). We recall that the eigenmodes of the one-body density matrix are distinct from those of the Hamiltonian, since the latter is not quadratic in the field.

The modes for $k \leq 30$ are shown for the system at $T = 1.3 T_\phi$ in the inset of Fig.15. The low-lying modes ($k < 10$) share a significant fraction of the total occupation; this is a consequence of the short-range phase coherence or quasi-condensation in the system, and similar to a “fragmented” condensate where many modes share a macroscopic occupation [9, 128]. A quantitative measure of how many modes contribute with a signif-

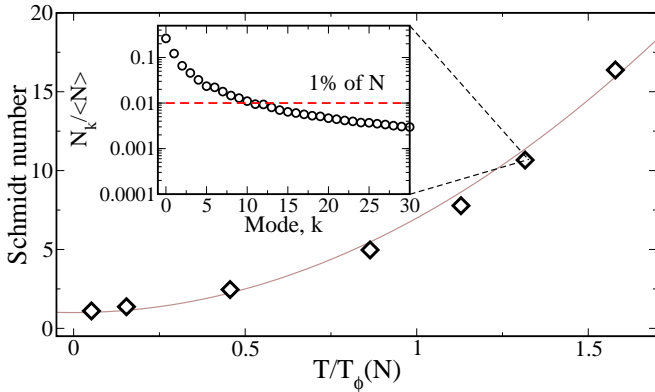


Figure 15: (Color online) Schmidt number versus scaled temperature for the sGPe simulations. Inset: at the temperature $T \approx 1.3 T_\phi$, the fractional occupation $N_k / \langle N \rangle$ for the 30 lowest modes with the largest occupation; condensate fraction (in $k = 0$ mode above) $\langle N_c \rangle / \langle N \rangle \approx 0.2$, and $\langle N \rangle \approx 23\,800$.

icant occupation can be given in terms of the Schmidt number S defined as [129]

$$S^{-1} = \sum_{k=0}^{\mathcal{M}} f_k^2 \quad (51)$$

where f_k is the fractional mode occupation given by

$$f_k = N_k / \sum_{k=0}^{\mathcal{M}} N_k. \quad (52)$$

The Schmidt number versus temperature extracted from sGPe simulations is shown in the main plot of Figure 15. In the limit of zero temperature, it tends towards 1: this is the signature of a pure Bose-Einstein condensate. For temperatures approaching T_ϕ , it increases quickly (a rather good fit is $S \approx 1 + 6(T/T_\phi)^2$, the black dotted line). At temperatures where the phase coherence length is shorter than the condensate size, one may expect a scaling $S \propto R(T)/L_\phi(T)$ which would be slower than linear. Modes outside the condensate region therefore contribute as well.

IV. CONDENSATION VS. QUASI-CONDENSATION

Due to the 1D nature of the system we consider, fluctuations in the density and phase are suppressed at different characteristic temperatures [3]. In this section, therefore, we highlight the distinction between the phase and density coherent portions of the gas, for which we will use the terminology “condensate” and “quasi-condensate”, respectively. This is an important problem in its own right, since stochastic theories (such as the sGPe [43, 51], or the pGPe [41]) automatically generate *total* densities of the field. The condensate mode is extracted from these either using bimodal fits (not commonly done, but experimentally well-known), or via the Penrose-Onsager (PO) prescription. This leads to a ‘gap’ between stochastic approaches and theories where a symmetry-breaking argument (or a variant of it) assigns a special “condensate mode” from the outset [22].

To investigate this issue further, we wish to establish here a more direct link between the PO condensate and the quasi-condensate often calculated in low-dimensional systems; we do this by directly comparing the PO mode of the sGPe data to the *ab initio* prediction of the modified Popov theory of Refs.[6, 7, 92] outlined in Sec.II E. As we shall show, this link has the advantage of providing an approximate PO condensate density without performing additional manipulations of the stochastic data like the diagonalization of the one-body density matrix.

A. Identifying the quasi-condensate

In Fig.16, we compare the quasi-condensate calculated from the modified Popov theory (within the local density approximation, see Sec.IIE) to the definition (53) below, based on the density correlation function (Sec.III C 2). In order to reveal the different physics contained in each of the approaches, in this figure, we have chosen a relatively high temperature ($T \approx 1.3 T_\phi \approx 0.63 T_c$) than for the previous comparison (chemical potential and interaction constant are kept the same). The breakdown of the ncB initial state in that regime constrains us to use only the sGPe stochastic data for this comparison. Due to the mapping between moments of

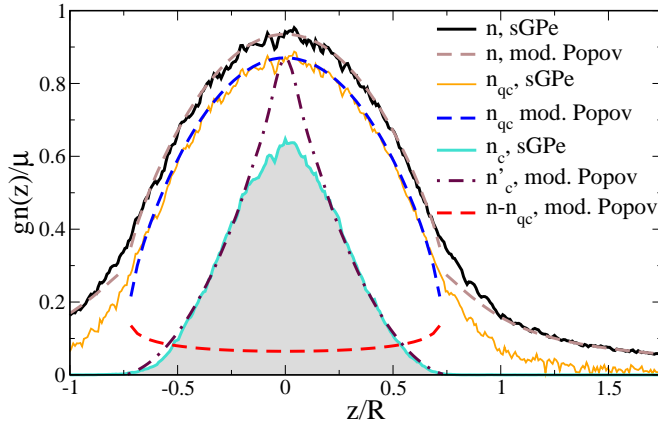


Figure 16: (Color online) Normalized density profiles showing: Total density (sGPe: Solid black, noisy; modified Popov: dashed, brown), quasi-condensate density (sGPe: solid orange, noisy; modified Popov: dashed, blue) and (phase coherent) condensate densities (sGPe PO: noisy, turquoise; modified Popov: dot-dashed/dotted, maroon). The modified Popov condensate density is shown dotted at small distances from the trap centre, where the relation $n'_c(z) = n_c(z)$ [see Eq.(56)] breaks down. The grey shaded region shows the Penrose-Onsager condensate density. The dashed red line shows $n(z) - n_{qc}(z)$ of the modified Popov theory. Here $T = 1.3 T_\phi = 0.63 T_c$ and $\langle N \rangle \approx 23800$. There are no ncB data because the ncB expansion no longer works at this temperature.

the Bose field operator to the stochastic field (Sec. II), one may extract a quasi-condensate density within these approaches in the following way

$$n_{qc}^2(z) = 2\langle \hat{\psi}^\dagger(z)\hat{\psi}(z) \rangle^2 - \langle \hat{\psi}^\dagger(z)\hat{\psi}(z)\hat{\psi}^\dagger(z)\hat{\psi}(z) \rangle. \quad (53)$$

This definition has been put forward in Ref.[130], and implemented in Refs.[116, 122]. Its equivalent form

$$n_{qc}(z) = n(z)\sqrt{2 - g^{(2)}(z)}, \quad (54)$$

has also been used at lower temperatures with the aim of extracting the (conventional) condensate mode in a 3D system [120], where phase fluctuations were

not expected to contribute significantly. The comparison of both the quasi-condensate (solid orange and dashed blue in Fig.16) and the total densities (solid black and dashed brown) between sGPe and modified Popov (respectively) gives very good agreement [64]. The quasi-condensate density profile is at this temperature clearly distinguishable from both the total density and the PO condensate (greyed area). The physical meaning of the quasi-condensate in modified Popov theory is thus that part of the system where density fluctuations are reduced such that $g^{(2)}(z) \approx 1$, as is typical for a single-mode coherent state. The plateau with $g^{(2)}(z) = 2$ outside the quasi-condensate in Fig.10 is, on the other hand, characteristic for a “chaotic” (or multi-mode) field [75, 125]. Note that this definition of the quasi-condensate is immune to phase fluctuations by construction [3]. Figure 16 shows that the density correlations obtained within the sGPe [Eq.(54)] indeed capture a quasi-condensate density consistent with that of Popov theory.

B. Identifying the Penrose-Onsager condensate density

The modified mean field theory of Andersen *et al.* [6, 7] splits the system into a quasi-condensate and other modes and thus avoids the “problem” of assuming the existence of long-range phase coherence. This makes the theory valid in arbitrary dimensions and at all temperatures. The approach can also capture the (conventional, PO) condensate mode by calculating the long-range limit of the one-particle density matrix [92] (see also Ref.[112]). In a homogeneous system, this leads to the definition

$$n_c = \lim_{x \rightarrow \infty} n_{qc} e^{-\frac{1}{2}\langle [\hat{\theta}(x) - \hat{\theta}(0)]^2 \rangle}. \quad (55)$$

This procedure recovers exactly the Popov results for quantum depletion in two and three dimensions, as pointed out in Ref.[92].

We wish to adapt Eq.(55) to the trapped case and construct the quantity

$$\begin{aligned} n'_c(z) &:= n_{qc}(z) e^{-\frac{1}{2}\langle [\hat{\theta}(z) - \hat{\theta}(0)]^2 \rangle} \\ &= n(z)\sqrt{2 - g^{(2)}(z)} g^{(1)}(0, z). \end{aligned} \quad (56)$$

We expect that this agrees well with the PO condensate density $n_c(z)$ for large $|z|$. As appears plausible on physical grounds, Eq.(56) involves a combination of density and phase correlation functions. This leads us to the second interesting feature of Fig.16: the density $n'_c(z)$ defined by Eq.(56) (dot-dashed and dotted, maroon) coincides, at large $|z|$, with the condensate density $n_c(z)$ obtained from the PO analysis of the one-body density matrix (solid light blue and shaded). This is important, as

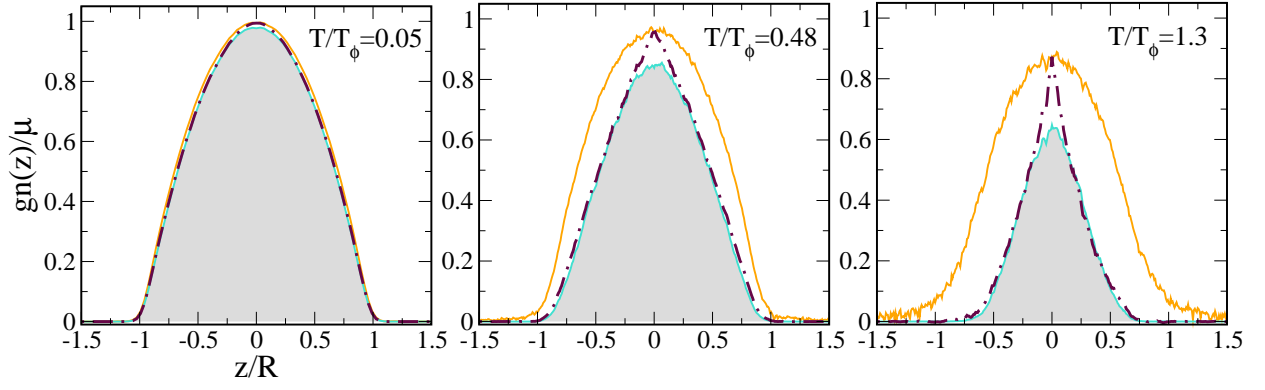


Figure 17: (Color online) Comparison between Eq. (56) (dot-dashed, maroon) and the PO mode due to diagonalizing the density matrix (solid turquoise and shaded) at three temperatures. Also shown is the quasi-condensate density from Eq.(54) (noisy orange curve), used to generate the dot-dashed maroon densities. The data here is extracted from the sGPe simulations.

it illustrates that the PO procedure produces a condensate that coincides with that fraction of atoms for which both phase and density fluctuations are reduced, i.e. the ‘true’ condensate. Equation (56) is also appealing from a practical point of view, as the extraction of the PO mode from stochastic data usually requires diagonalization of the one-body density matrix, which for very large systems can become a significant computational task. In contrast, the correlation functions $g^{(1)}(0, z)$ and $g^{(2)}(z)$ that enter Eq.(56) are very straightforward to calculate, making the analysis much quicker.

The condensate density predicted by Eq.(56) agrees well with the one obtained by Penrose-Onsager analysis also for a range of temperatures, as shown in Fig.17. This figure also illustrates how the distinction between quasi-condensate and PO condensate becomes more noticeable as $T \sim T_\phi$. For all temperatures, Eq.(56) gives a good approximation to the PO density, with an increasing difference evident only in the central region of the trap. The size of this region at $T = 1.3T_\phi$ corresponds roughly to the extent over which the non-condensate part of $g^{(1)}(z)$ is positively correlated (see Eq.(43) and the dot-dashed red curve in Fig. 9(d)). The origin of the ‘spike’, then, lies in the fact that the thermal component is coherent over this small region too, so it is not just the condensate which contributes to $g^{(1)}(z)$ at short scales. Again from Fig. 9, it is interesting to note that the non-condensate contribution to $g^{(1)}(z)$ is actually significant at larger $|z|$ where it reduces the condensate contribution (dashed blue curve).

C. Application: (quasi) condensate fraction

To test the reliability of the condensate density suggested in Eq.(56), we have calculated the fraction of atoms in the (quasi-) condensate over a range of temperatures. The data are shown in Fig.18. The two upper

curves give the quasi-condensate fraction which is systematically larger. At low temperatures, $T \ll T_\phi$, condensate and quasi-condensate numbers are very similar, as already noted in [44, 116, 131]. In this range, we also get a good agreement between stochastic data and the modified Popov theory. As T increases towards T_ϕ , however, the deviation between condensate and quasi-condensate increases. This is clearly due to the shrinking of the PO condensate at its borders, as seen in Fig.17. The difference among the two (PO) condensate numbers is due to the central “spike” that follows from Eq.(56):

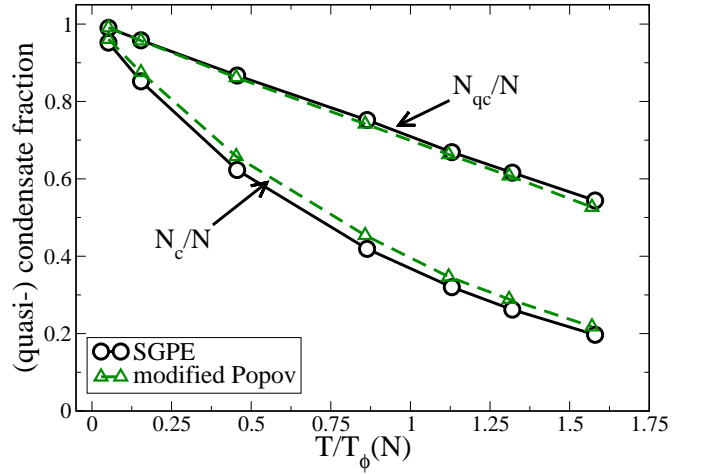


Figure 18: (Color online) (1d) Quasi-condensate and PO condensate numbers from the sGPe (black circles) and modified Popov theory (hollow green triangles). The sGPe results are based on the condensate mode given by PO analysis of the one-body density matrix (Sec.III B) and on Eq.(53) for the quasi-condensate. For the integration over $n_{qc}(z)$, only the region $|z| \leq R(T)$ is taken into account. The modified Popov data are based on the quasi-condensate density described in Sec.IIE and on the condensate density $n'_c(z)$ given in Eq.(56), where $g^{(1)}(0,z)$ is calculated from Eq.(40).

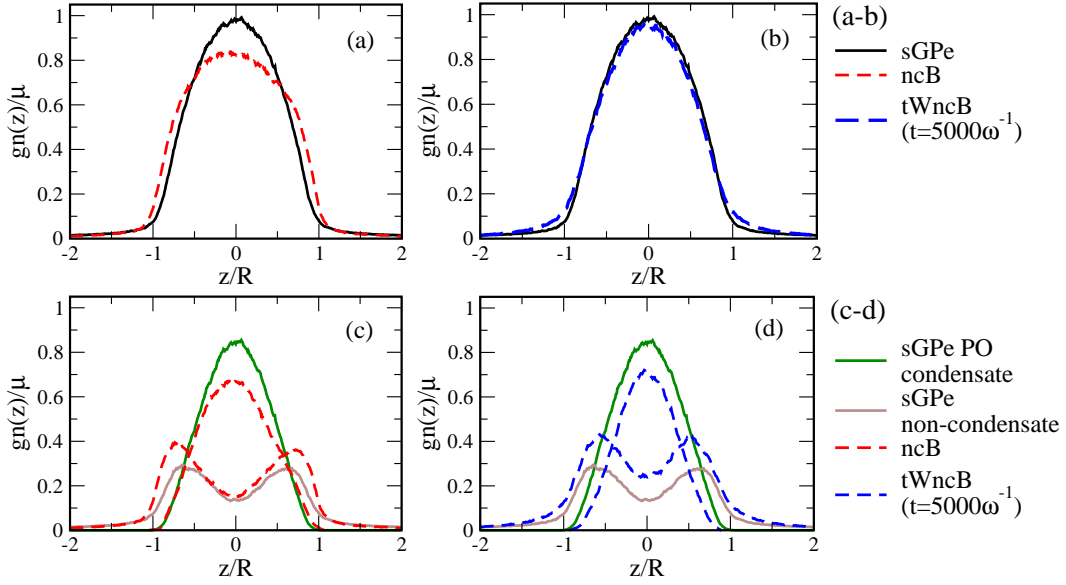


Figure 19: (Color online) Top row (a, b): total atomic density for the sGPe (solid, black) at equilibrium and tWncB (a) before (dashed red) and (b) after (dashed blue) evolution via the GPe. The tWncB data contain the correction to normal order; the evolution period is $5000\omega^{-1}$. Bottom row (c, d): condensate/thermal density (sGPe:solid green/brown; tWncB: dashed), as obtained by Penrose-Onsager analysis [see Fig.7], (c) before (dashed red) and (d) after (dashed blue) evolution of the ncB state over $5000\omega^{-1}$. Upper curves: condensate density, lower curves with maxima at $|z| \lesssim R$: thermal density.

at $z = 0$, one has necessarily $g^{(1)}(0) = 1$ and $n'_c(0) = n_{qc}(0)$, but diagonalizing the one-body density matrix of the sGPe data yields $n_c(0) < n_{qc}(0)$ [Fig.17]. Despite this difference, the two condensate numbers agree relatively well and show the same qualitative temperature dependence.

The approximate condensate density $n'_c(z)$ of Eq.(56) can be evaluated in a simpler way by using Eq.(40) for the calculation of the phase correlation function $g^{(1)}(0, z)$. This means in practice that one only needs to extract the parameter $R(T)$ from the modified Popov density profiles. We have already shown in Fig.9(d) that this simplified expression works well to approximate $g^{(1)}(0, z)$.

V. SLOW THERMALIZATION OF THE INITIAL STATE

We have seen the importance of a consistent treatment of phase and density fluctuations in calculating accurately a finite-temperature initial state for our (quasi)-one-dimensional system. From the physical observables probed, the picture emerging so far is that equilibrium properties, like total densities, agree quite well over a range of temperatures well beneath T_ϕ and in the spatial range where highly occupied modes are dominant. The stochastic ensembles prepared by the two methods are considered in this section as an initial condition for the Gross-Pitaevskii equation, which will be used to describe the subsequent dynamics. We take a tempera-

ture $\approx 0.48 T_\phi$ where the ncB data is clearly not in equilibrium, and address the question whether these data evolve dynamically into a thermal equilibrium state. We shall find that even after a fairly long evolution time ($> 5000\omega^{-1}$), the system is not yet stationary. This may be related to the absence of thermalization in integrable homogeneous 1D systems [108, 109, 132, 133].

The thermalization study presented here provides a link to other classical field methods. These approaches, for example the pGPe of Davis, Blakie and co-workers [41], that employed by Berloff and Svistunov [54] and the approach of the Polish group [59], typically use a single field realization with suitably randomized initial conditions as an input to evolution under the GPe (with the possible addition of a projector [53]), rather than an ensemble of initial states. The system then corresponds to a microcanonical ensemble, as both particle number and total energy are fixed in this scenario. The dynamics acquires an irreversible character by spatial or temporal coarse-graining [134]. This can be mapped to a Boltzmann equation that yields an irreversible evolution where the system thermalizes to an equilibrium state with Rayleigh-Jeans statistics [41, 135].

Figure 19 shows the density profile and its resolution into condensate and thermal density, before (left panels) and after (right panels) GPe evolution. While the total densities (top row) agree well between the two methods, the ncB data evolve towards a smaller condensate density (bottom row), suggesting the system to be thermalized at a higher temperature.

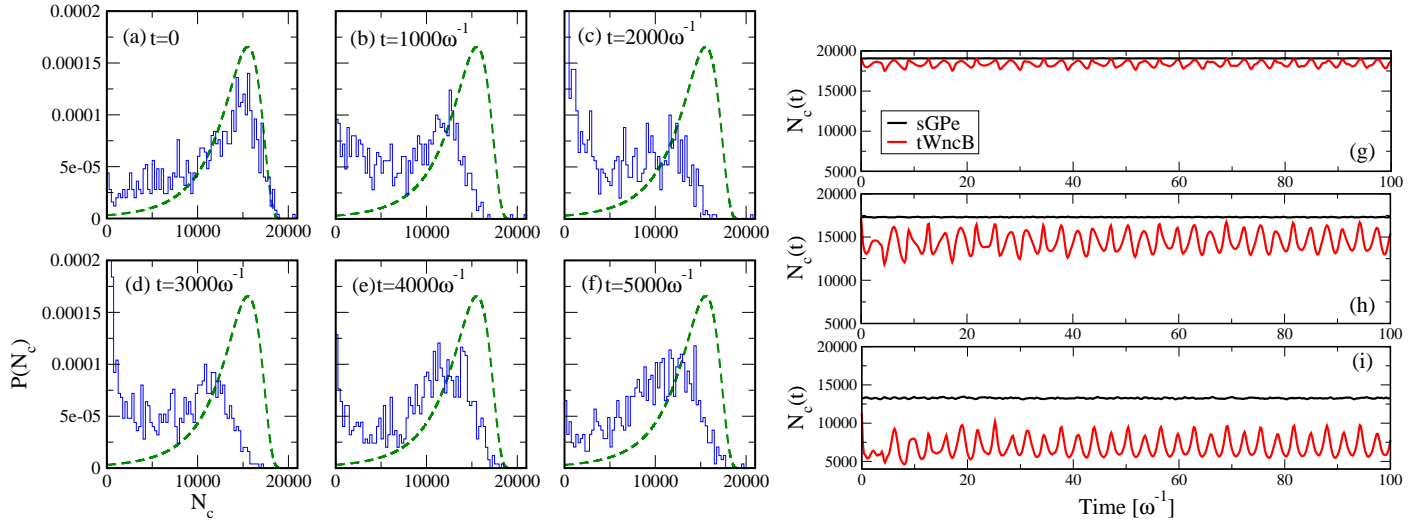


Figure 20: (Color online) Left: condensate statistics at different evolution times under the GPe, at initial nominal temperature $T \approx 0.48 T_\phi$. Solid blue: tWncB data, dashed green: equilibrium S&co theory [71]. The sGPe data at equilibrium are not shown, as the condensate statistics essentially stays the same as in Fig.13. Right: mean condensate statistics $\langle N_c(t) \rangle$ for sGPe (upper, black line), tWncB (lower, red curve) at the temperatures of Table II, with temperature increasing from top (g) to bottom (i).

The temporal evolution of the condensate statistics is illustrated in Fig. 20 (left). This data was extracted as follows: we obtain the one-body density matrix at the indicated times and get the condensate mode by Penrose-Onsager diagonalization. Projecting the ensemble of wave functions onto this mode, one gets a few snapshots of the evolving condensate statistics $P(N_c, t)$. While this distribution shows essentially no variation for the sGPe initial data, the ncB case shows a significant evolution. The peak at $\langle N_c \rangle$ disintegrates quite rapidly, and the condensate is re-formed gradually, with a broader peak re-appearing from smaller to higher numbers. At the final time, the distribution does yet not appear to have reached a stable distribution.

The right panel in Fig. 20 illustrates that over short time scales, the average condensate number oscillates for the ncB data, in contrast to the sGPe (note the shorter time scale compared to the left panels, in order to resolve the oscillations in the ncB data). This oscillation at roughly 2ω , whose amplitude increases with temperature, may be due to a nonlinear locking between the condensate mode and its low-lying, highly excited excitations.

The evolution of the coherence functions is illustrated in Fig.21 for the $g^{(1)}$ and $g^{(2)}$ functions introduced in Secs.III C 1, III C 2. The kinks in Fig. 21(a) could be due to a mode coupling between the condensate and low-energy excitations whose mode functions have nodes and are slightly broader. But it is unclear whether this picture may explain the strong density fluctuations (panel (d)). The average density is quite low for $|z| > R$, which amplifies sampling errors, however.

Recalling the discussion in Secs.III C 1, III C 2 [Eqs.(42)

and (46)], we can use the correlation functions to measure the temperature of the ensemble. This may not yield a consistent picture, since the system is not (yet) thermalized. At least, we can place bounds on the temperature range that the system might thermalize to, albeit after some longer time. The results of this are summarized in Fig. 22. We probe the system properties at non-constant time intervals, in order to account for the possibility of periodic behaviour in the correlation functions. For example, the last two data points on the upper curve are separated by only $10 \omega^{-1}$ units of time. The lower dashed red line indicates the input temperature ($0.48 T_\phi$), but both $g^{(1)}$ and $g^{(2)}$ yield higher numbers. Notice that $g^{(1)}$ gives a higher temperature, as might be expected in our regime due to pronounced phase fluctuations. The temperature extracted from $g^{(2)}$ is more stable in time, which may suggest a faster damping rate for modes with density fluctuations. This would be consistent with Landau-Beliaev damping, see, e.g., Refs.[38, 59].

To summarize this discussion, we emphasize that in this example thermalization proceeds quite slowly. The 1D character of the system that is nearly integrable probably plays a role here, but also relevant are the large fluctuations that are present in the initial state produced by the ncB method. One may think of the $1/2$ “quantum atoms” per mode that are included in the truncated Wigner sampling: the observed temperature increase is roughly comparable to the “classical thermalization” of these atoms, as simple estimates show [38]. The different temperatures extracted from phase and density correlations, however, are probably related to the wrong account of phase fluctuations: they are mis-interpreted in

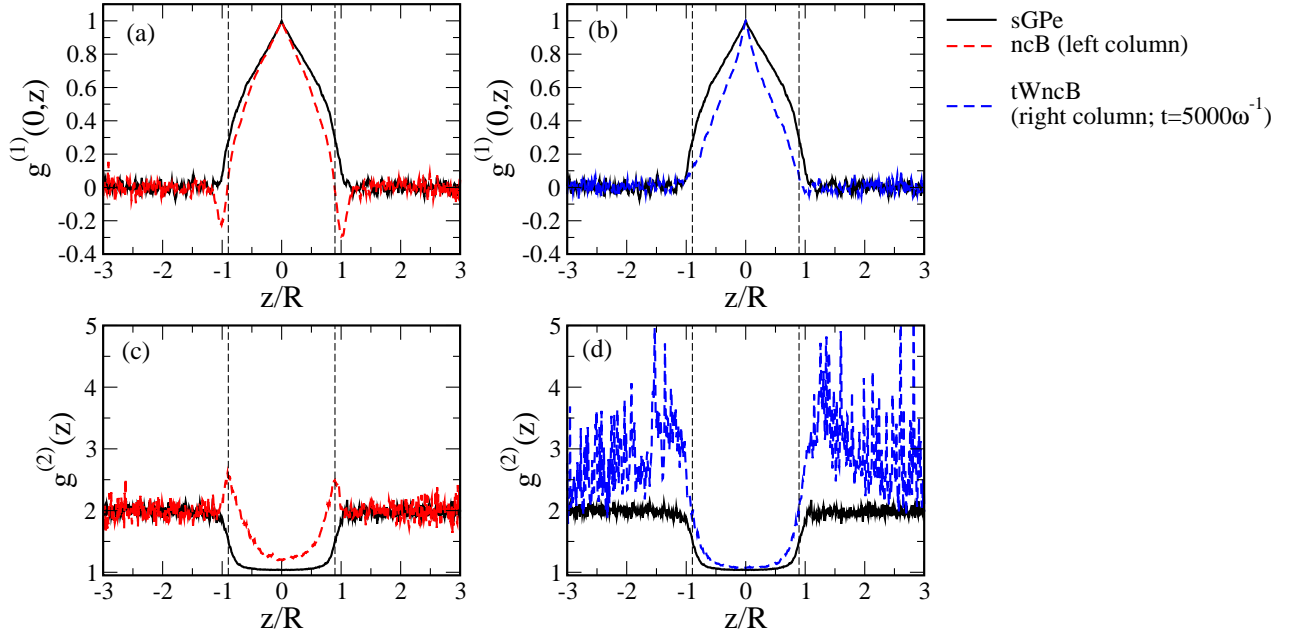


Figure 21: (Color online) Top row: $g^{(1)}(z)$ for the sGPe (solid black), (a) tWncB initially at ($t = 0$) (dashed red) and (b) tWncB after GPe evolution up to $t = 5000\omega^{-1}$ (dashed blue); bottom row: as per top row for $g^{(2)}(z)$. In each plot, the vertical dashed line indicates $R(T)$ at $T = 430\hbar\omega$.

terms of non-condensate density, as illustrated in Fig.12. This may be cured by formulating the stochastic scheme in terms of phase and density variables, instead of the non-condensate field $\psi_{\perp}(z)$, similar to the analysis of Ref.[39].

VI. CONCLUSIONS

We have analyzed the equilibrium properties of a weakly interacting, trapped quasi-one-dimensional Bose gas at finite temperatures, which we modelled as

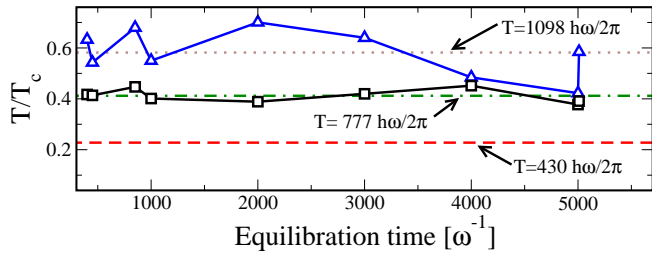


Figure 22: (Color online) Temperature measurement using correlation functions as a function of GPe evolution time: (upper data) $g^{(1)}(z)$, for $0 < z < R/2$ and Eq. (42) (blue triangles); (lower data) $g^{(2)}(0)$ and Eq. (46) (black squares). Initial temperature (dashed red); Best horizontal fit through $g^{(1)}(z)$ data (dotted brown) and through $g^{(2)}(0)$ data (dot-dashed green); temperatures corresponding to the horizontal lines are indicated.

an effective one-dimensional system. The predictions of a number of independent finite-temperature theories have been compared. We focussed in particular on two methods incorporating phase and density fluctuations in a stochastic manner: a number conserving Bogoliubov approach with stochastic sampling and the stochastic Gross-Pitaevskii equation.

At low temperatures, we found average quantities, such as total density profiles, condensate fractions and first and second order spatial correlation functions to give good agreement between the two theories. These properties were additionally found to coincide with other theoretical predictions from the literature, which we used in order to ‘benchmark’ our findings. As higher temperatures were probed, though still within the regime $T < T_{\phi}$, the ncB initial state was found to give predictions for equilibrium properties in disagreement with both the sGPe and the results of other, ‘benchmark’ theories, including the modified Popov theory of [6], while the latter two showed good agreement. We attribute this failure to the use of the $T = 0$ Bogoliubov spectrum in the ncB expansion, i.e. the condensate number is assumed equal to the total particle number at all temperatures, and to the overestimation of the non-condensate density due to spurious contributions of phase fluctuations at higher orders. The ‘point cloud’ in Fig. 12 illustrates the enhanced phase fluctuations at higher temperatures, which mean that density fluctuations in modes above the condensate were no longer suppressed in the ncB method, as would be expected at

temperatures much below the ‘degeneracy’ temperature (T_d). A procedure taking condensate depletion into account in a temperature dependent way, would likely improve the high-temperature behaviour of this method.

We have also probed quantities involving higher-order statistical moments than just the density or its correlation, in particular the full distribution function of the condensate number. At low temperatures, and for not too small atom numbers (where the assumption of a ‘classical’ occupation of modes fails), both ncB and sGPe were found to produce the correct statistics, in perfect agreement to the theory of Svidzinsky and Scully [71]. However, for small total particle numbers, and at low temperature, the sGPe results were found to be broader than the ncB statistics, whereas the latter were found to agree well with those of Ref. [71]. The incorrect sGPe prediction at low particle numbers was attributed to the onset of anomalously large number fluctuations, familiar from the grand-canonical analysis of the ideal gas. As the importance of interactions within the system was increased, i.e. by increasing particle number with all other parameters fixed, the sGPe and Svidzinsky and Scully results were then found to match well.

We further propagated the ncB data via the (ordinary) GPe, as done in the truncated Wigner approach. We found that this leads to the correct profiles for the total system density, but fails to predict all other features accurately, due to its attempt to thermalize to a higher temperature classical field. This thermalisation was found to take extremely long here, due to our 1d system configuration.

Finally, we have illustrated the conceptual difference between the (phase-coherent) condensate and the (density-coherent) quasi-condensate. The former is usually obtained by the Penrose-Onsager analysis of the one-body density matrix while the latter appears e.g. in the context of the modified Popov theory of Refs.[6, 7]. Building on the identification of the (PO) condensate for a homogeneous system [92], we have provided an alternative, numerically very efficient means of extracting information about the condensate density that involves only first- and second-order correlation functions, as obtained from the sGPe simulations. Although some issues remain to be improved near the trap centre, condensate density and fraction are perfectly matched to the conventional PO approach over a broad range of parameters. We believe that this identification, along with the systematic benchmarking of observables to alternative theories for finite- T Bose gases will provide a better understanding of the links between stochastic theories and thermodynamics based on mean field theories.

Acknowledgments. We acknowledge financial support from the EPSRC (SPC, NPP), the Lundbeck Foundation (AN), the Deutsche Forschungsgemein-

schaft within the grants SFB/TRR21 (AN) and He-2849/3 (CH), the Marie Curie Intra-European Fellowship within the 7th European Community Framework Programme (AN), and the Forschungsbonus der Universität Ulm und der Ulmer Universitätsgesellschaft (AN). AN acknowledges fruitful discussions with A. Sinatra, Y. Castin, U. V. Poulsen, and I. Carusotto on the truncated Wigner method. NPP acknowledges stimulating discussions with Matt Davis, Allan Griffin, Tod Wright and Eugene Zaremba on the links between ‘classical field’ and kinetic equations based on symmetry-breaking. CH thanks M. Abel for inspiring comments.

Appendix A: Sampling the number-conserving Bogoliubov state

The condensate mode function $\phi_c(z)$ contains two terms

$$\phi_c(z) = \frac{\phi_0(z) + \phi_2(z)/N}{(1 + \|\phi_2(z)/N\|^2)^{1/2}}, \quad (\text{A1})$$

that arise in zero’th and second order of the expansion. The lowest-order contribution $\phi_0(z)$ solves the stationary GPe

$$H_{\text{GP}}[N|\phi_0|^2]\phi_0 = \mu\phi_0. \quad (\text{A2})$$

Note that the ‘chemical potential’ μ emerges here as the lowest eigenvalue of a nonlinear eigenproblem: it depends on the product gN and the trapping potential $V(z)$. Equation (A2) is conveniently solved by propagating the wave function in imaginary time.

For the correction $\phi_2(z)$, one needs the non-condensate field $\psi_\perp(z)$, and we return to it in Eq.(A8). The non-condensate atoms populate Bogoliubov mode functions $u_k(z)$ and $v_k(z)$. These are eigenfunctions of the (projected) Bogoliubov–de Gennes operator

$$\mathcal{L}_Q = \begin{pmatrix} Q & 0 \\ 0 & Q^* \end{pmatrix} \mathcal{L} \begin{pmatrix} Q & 0 \\ 0 & Q^* \end{pmatrix} \quad (\text{A3})$$

$$\mathcal{L} = \begin{pmatrix} H_{\text{GP}}[2N|\phi_0|^2] - \mu & gN\phi_0^2 \\ -gN\phi_0^{*2} & -H_{\text{GP}}[2N|\phi_0|^2] + \mu \end{pmatrix} \quad (\text{A4})$$

where Q (Q^*) is the projector orthogonal to $\phi_0(z)$ (to $\phi_0^*(z)$), respectively. On the spatial grid, its matrix elements are

$$Q_{zz'} = \delta_{zz'} - \Delta z \phi_0(z) \phi_0^*(z'). \quad (\text{A5})$$

The numerical diagonalization of \mathcal{L}_Q may be approached simply with a Fourier grid method [136], for example. We need in Eq.(6) only those modes with $\epsilon_k > 0$ that can be normalized to

$$\Delta z \sum_z [u_k^*(z)u_l(z) - v_k^*(z)v_l(z)] = \delta_{kl} \quad (\text{A6})$$

where the sum represents the Bogoliubov scalar product on the spatial grid (spacing Δz). For a grid of length L , the number of Bogoliubov modes is $\mathcal{M} = L/\Delta z - 1$.

The quantity $\mathcal{A}(\{b_k\})$ in Eq.(9) is calculated as

$$\begin{aligned} \mathcal{A}(\{b_k\}) = & \sum_k \frac{|b_k|^2 - \sigma_k^2}{4\sigma_k^4} + \sum_{k,q} \frac{\Delta z}{2\sigma_k^2\sigma_q^2} \times \\ & \sum_z \{ \text{Re}(b_k b_q^* - \delta_{kq}\sigma_k^2)v_k^*(z)v_q(z) \\ & - \text{Re}(b_k b_q)u_k^*(z)v_q(z) \}, \end{aligned} \quad (\text{A7})$$

where σ_k^2 is the expectation value of $|b_k|^2$, so that $\mathcal{A}(\{b_k\})$ averages to zero. This term encodes the Wigner correction for getting the (normally ordered) non-condensate particle number out of the semiclassical Wigner functions, at the level of the corresponding number variances.

The second-order correction $\phi_2(z)$ to the condensate mode $\phi_0(z)$ is due to thermal depletion. It contributes in the ncB expansion at the same order as the non-condensate modes to typical observables like the average density and the one-body density matrix. It must be orthogonal to $\phi_0(z)$ (see [80]) and can hence be expanded over the Bogoliubov modes

$$\phi_2(z) = \sum_k [c_k u_k(z) + c_k^* v_k^*(z)]. \quad (\text{A8})$$

The coefficients c_k are found by solving an inhomogeneous linear equation for the Bogoliubov-de Gennes operator. For the convenience of the reader, we reproduce here Eqs.(71)-(75) provided in Ref.[46]. The Wigner field ψ_\perp represents a non-condensate field operator denoted $\hat{\Lambda}$ in Ref.[46]. The second-order correction ϕ_2 solves the stationary equation

$$\mathcal{Q}(H_{\text{GP}}[2N|\phi_0|^2] - \mu)\phi_2 + gN\mathcal{Q}\phi_0^2\phi_2^* = -\mathcal{Q}R \quad (\text{A9})$$

with a “source term”

$$\begin{aligned} R(x) = & -gN|\phi_0(x)|^2\phi_0(x)(1 + \langle\hat{N}_{\text{th}}\rangle) \\ & + 2gN\langle\hat{\Lambda}^\dagger(x)\hat{\Lambda}(x)\rangle\phi_0(x) + gN\phi_0^*(x)\langle\hat{\Lambda}(x)\hat{\Lambda}(x)\rangle \\ & - gN \int dy |\phi_0(y)|^2 \langle(\hat{\Lambda}^\dagger(y)\phi_0(y) + \phi_0^*(y)\hat{\Lambda}(y))\hat{\Lambda}(x)\rangle \end{aligned} \quad (\text{A10})$$

where $\hat{N}_{\text{th}} = \int dx \hat{\Lambda}^\dagger(x)\hat{\Lambda}(x)$ is the operator for the non-condensate atom number. The expectation values of $\hat{\Lambda}$ are translated into Wigner averages of ψ_\perp according to the symmetrization rule

$$\langle\hat{\Lambda}^\dagger(x)\hat{\Lambda}(x')\rangle = \langle\psi_\perp^*(x)\psi_\perp(x')\rangle_W - \frac{1}{2}\mathcal{Q}(x, x') \quad (\text{A11})$$

where the projector $\mathcal{Q}(x, x')$ appears because the fields live in the subspace orthogonal to the zero'th order condensate mode $\phi_0(z)$. Equation (A9) is solved by

constructing an imaginary time evolution that leads to $\phi_2(z)$ as a stationary solution. This is then plugged into Eq.(A1) to complete the construction of the normalized condensate mode $\phi_c(z)$.

With this normalisation, the stochastic matter wave field $\psi(z)$ gives access to the total particle density $n(z)$ as [cf. Eq.(3)]

$$n(z) = \langle|\psi(z)|^2\rangle_W - n_q \quad (\text{A12})$$

where n_q is the quantum density (4). It is hence normalized such that $\langle\|\psi\|^2\rangle_W = N + \mathcal{M}/2$. The statistics of the condensate atom number N_c is determined by the non-condensate field ψ_\perp , via Eq.(9).

The propagation in time of the matter field $\psi(z, t)$ is found by solving the GPe (2). This turns out to be more accurate, in particular at long times, than to propagate separately the condensate mode and ψ_\perp , using the time-dependent versions of the equations they solve in the respective orders of the expansion in $(\delta N/N)^{1/2}$ (see, e.g., [37]). All numerical simulations in this paper (for both methods) are based on the Crank-Nicholson method for time stepping with the results averaged over at least 1000 realisations of the initial conditions.

Appendix B: Canonical counting statistics of a Bose gas

The group of Scully and co-workers (S&Co) has developed theoretical models to calculate the counting statistics $P(N_c)$ of a Bose condensate, building on the canonical ensemble where the operators \hat{N}_c and \hat{N}_{th} must sum up to the (fixed) total number N . Therefore, the counting statistics is the “mirror image” of the probability distribution $P(N_{\text{th}})$. The latter can be calculated when the non-condensate number \hat{N}_{th} splits into a sum of statistically independent terms. In an ideal Bose gas, this would be the occupation numbers \hat{n}_k of single-particle modes (quantum number k). For a weakly interacting, homogeneous Bose gas, the non-condensate atoms are clearly those in non-zero momentum modes, and hence

$$\begin{aligned} \hat{N}_{\text{th}} = & \sum_{p>0} \{(u_p^2 + v_p^2)(\hat{b}_p^\dagger\hat{b}_p + \hat{b}_{-p}^\dagger\hat{b}_{-p}) \\ & + 2u_p v_p(\hat{b}_p^\dagger\hat{b}_{-p}^\dagger + \hat{b}_p\hat{b}_{-p}) + 2v_p^2\} \end{aligned} \quad (\text{B1})$$

where u_p and v_p are real-valued Bogoliubov coefficients [Eq.(258) of Ref.[70]], normalized to $u_p^2 - v_p^2 = 1$, and where the \hat{b}_p are the bosonic operators for Bogoliubov quasi-particles. This Bogoliubov spectrum depends on the condensate occupation number N_c . S&Co make the approximation that the dependence is weak enough so that N_c can be replaced by its average value $\langle N_c \rangle$ (i.e., by the first moment of $P(N_c)$). This is consistent if $P(N_c)$ is narrow enough. The operator identity (B1) is also

based on the assumption of a negligibly small probability $P(N_c = 0)$ of finding the condensate mode empty [Eq.(210) of Ref.[70]].

The quasi-particle operators are constructed such that the sum (B1) contains mutually commuting operators (only momenta p and $-p$ are correlated), and the probability distribution $P(N_{\text{th}})$ can be found with standard techniques. The following moments are found, for example

$$\langle N_{\text{th}} \rangle = \sum_{p \neq 0} \{ \bar{N}_p u_p^2 + (\bar{N}_p + 1) v_p^2 \} \quad (\text{B2})$$

$$\sigma^2(N_{\text{th}}) = \sum_{p \neq 0} \{ \bar{N}_p (\bar{N}_p + 1) [1 + 8u_p^2 v_p^2] + 2u_p^2 v_p^2 \} \quad (\text{B3})$$

$$\begin{aligned} \mu_3 = & - \sum_{p \neq 0} (u_p^2 + v_p^2) \{ \bar{N}_p (2\bar{N}_p^2 + 3\bar{N}_p + 1) \\ & \times [1 + 16u_p^2 v_p^2] + (2\bar{N}_p + 1) 4u_p^2 v_p^2 \} \end{aligned} \quad (\text{B4})$$

where $\bar{N}_p = \bar{N}(\epsilon_p)$ is the Bose-Einstein statistics and where $\mu_3 = \langle (\hat{N}_{\text{th}} - \langle \hat{N}_{\text{th}} \rangle)^3 \rangle$ is the third central moment. Its nonzero value is a clear indication of non-Gaussian statistics. These results are obtained within the Bogoliubov approximation with a weak thermal fraction, $\langle N_{\text{th}} \rangle \ll N$, hence at low temperatures.

Svidzinsky and Scully [71] have generalized this approach to any temperature, using a rate equation *Ansatz* similar to quantum laser theory [74]. The growth and loss rates for the condensate depend on N_c and are described by a rational (Padé) approximation. This leads to a closed formula for the stationary $P(N_c)$. The Padé parameters are matched to the low-temperature limit and can be expressed in terms of the moments (B2–B4). The equation $\langle N_c \rangle = N - \langle N_{\text{th}} \rangle$ must be solved iteratively since the Bogoliubov modes in Eq.(B2) depend themselves on $\langle N_c \rangle$. It has been pointed out in Ref.[72] that the dependence of the Bogoliubov spectrum on the condensate number, $\epsilon_p(N_c) \neq \epsilon_p(\langle N_c \rangle)$, actually leads to an observable difference in the counting statistics, although it makes the calculations much more involved.

We calculate the counting statistics in Figs.13, 14 using the theory of Ref.[71] and making the identification $u_p^2 \mapsto \|u_k\|^2$ to the Bogoliubov modes in a trap. The moments of $P(N_c)$ in Fig.14 are calculated from Eqs.(B2–B4).

-
- [1] C. J. Pethick and H. Smith, *Bose-Einstein Condensation in Dilute Gases* (Cambridge University Press, Cambridge, 2002).
 - [2] L. P. Pitaevskii and S. Stringari, *Bose-Einstein Condensation*, vol. 116 of *International Series of Monographs on Physics* (Oxford University Press, Oxford New York, 2003).
 - [3] V. N. Popov, *Functional Integrals in Quantum Field Theory and Statistical Physics* (Reidel, Dordrecht, 1983), chap. 6.
 - [4] D. S. Petrov, G. V. Shlyapnikov, and J. T. M. Walraven, *Phys. Rev. Lett.* **85**, 3745 (2000).
 - [5] Y. Kagan, V. A. Kashurnikov, A. V. Krasavin, N. V. Prokof'ev, and B. Svistunov, *Phys. Rev. A* **61**, 043608 (2000).
 - [6] J. Andersen, U. A. Khawaja, and H. Stoof, *Phys. Rev. Lett.* **88**, 070407 (2002).
 - [7] U. A. Khawaja, J. O. Andersen, N. P. Proukakis, and H. T. C. Stoof, *Phys. Rev. A* **66**, 013615 (2002), erratum: *Phys. Rev. A* **66**, 059902(E) (2002).
 - [8] C. Gies, B. P. van Zyl, S. A. Morgan, and D. A. W. Hutchinson, *Phys. Rev. A* **69**, 023616 (2004).
 - [9] A. J. Leggett, *Rev. Mod. Phys.* **73**, 307 (2001).
 - [10] N. P. Proukakis, K. Burnett, and H. T. C. Stoof, *Phys. Rev. A* **57**, 1230 (1998).
 - [11] H. Shi and A. Griffin, *Physics Reports* **304**, 1 (1998).
 - [12] O. J. Luiten, M. W. Reynolds, and J. T. M. Walraven, *Phys. Rev. A* **53**, 381 (1996).
 - [13] D. Jaksch, C. W. Gardiner, and P. Zoller, *Phys. Rev. A* **56**, 575 (1997).
 - [14] M. Holland, J. Williams, and J. Cooper, *Phys. Rev. A* **55**, 3670 (1997).
 - [15] E. Zaremba, T. Nikuni, and A. Griffin, *J. Low Temp. Phys.* **116**, 277 (1999).
 - [16] R. Walser, J. Williams, J. Cooper, and M. Holland, *Phys. Rev. A* **59**, 3878 (1999).
 - [17] M. J. Bijlsma, E. Zaremba, and H. T. C. Stoof, *Phys. Rev. A* **62**, 063609 (2000).
 - [18] C. W. Gardiner and P. Zoller, *Phys. Rev. A* **61**, 033601 (2000).
 - [19] N. P. Proukakis, *J. Phys. B: At. Mol. Opt. Phys.* **34**, 4737 (2001).
 - [20] T. R. Kirkpatrick and J. R. Dorfman, *Phys. Rev. A* **28**, 2576 (1983).
 - [21] U. Eckern, *J. Low Temp. Phys.* **54**, 333 (1984).
 - [22] A. Griffin, T. Nikuni, and E. Zaremba, *Bose-Condensed Gases at Finite Temperatures* (Cambridge University Press, Cambridge, 2009).
 - [23] T. Nikuni, E. Zaremba, and A. Griffin, *Phys. Rev. Lett.* **83**, 10 (1999).
 - [24] T. Nikuni and A. Griffin, *Phys. Rev. A* **63**, 033608 (2001).
 - [25] B. Jackson and E. Zaremba, *Phys. Rev. Lett.* **87**, 100404 (2001).
 - [26] B. Jackson and E. Zaremba, *Phys. Rev. Lett.* **88**, 180402 (2002).
 - [27] B. Jackson and E. Zaremba, *Phys. Rev. Lett.* **89**, 150402 (2002).
 - [28] B. Jackson, N. P. Proukakis, and C. F. Barenghi, *Phys. Rev. A* **75**, 051601 (2007).
 - [29] B. Jackson, N. P. Proukakis, C. F. Barenghi, and E. Zaremba, *Phys. Rev. A* **79**, 053615 (2009).
 - [30] A. Griffin, *Phys. Rev. B* **53**, 9341 (1996).
 - [31] N. P. Proukakis, S. A. Morgan, S. Choi, and K. Burnett, *Phys. Rev. A* **58**, 2435 (1998).
 - [32] D. A. W. Hutchinson, K. Burnett, R. J. Dodd, S. A. Morgan, M. Rusch, E. Zaremba, N. P. Proukakis, M. Edwards, and C. W. Clark, *J. Phys. B* **33**, 3825 (2000).
 - [33] P. Tommasini, E. J. V. de Passos, M. O. C. Pires, and A. F. R. de Toledo Piza, *J. Phys.: Condens. Matt.* **17**, 3165 (2005).
 - [34] V. I. Yukalov and H. Kleinert, *Phys. Rev. A* **73**, 063612 (2006).
 - [35] U. Al Khawaja, N. P. Proukakis, J. O. Andersen, M. W. J. Romans, and H. T. C. Stoof, *Phys. Rev. A* **68**, 043603 (2003).
 - [36] N. P. Proukakis, *Phys. Rev. A* **73**, 023605 (2006).
 - [37] A. Sinatra, C. Lobo, and Y. Castin, *Phys. Rev. Lett.* **87**, 210404 (2001).
 - [38] A. Sinatra, C. Lobo, and Y. Castin, *J. Phys. B* **35**, 3599 (2002).
 - [39] C. Mora and Y. Castin, *Phys. Rev. A* **67**, 053615 (2003).
 - [40] B. Svistunov, *J. Moscow Phys. Soc.* **1**, 373 (1991).
 - [41] M. J. Davis, S. A. Morgan, and K. Burnett, *Phys. Rev. Lett.* **87**, 160402 (2001).
 - [42] K. Góral, M. Gajda, and K. Rzążewski, *Phys. Rev. A* **66**, 051602(R) (2002).
 - [43] H. T. C. Stoof, *J. Low Temp. Phys.* **114**, 11 (1999).
 - [44] P. B. Blakie and M. J. Davis, *Phys. Rev. A* **72**, 063608 (2005).
 - [45] M. J. Steel, M. K. Olsen, L. I. Plimak, P. D. Drummond, S. M. Tan, M. J. Collett, D. F. Walls, and R. Graham, *Phys. Rev. A* **58**, 4824 (1998).
 - [46] A. Sinatra, Y. Castin, and C. Lobo, *J. Mod. Opt.* **47**, 2629 (2000).
 - [47] A. Polkovnikov, *Phys. Rev. A* **68**, 053604 (2003).
 - [48] H. T. C. Stoof and M. J. Bijlsma, *J. Low Temp. Phys.* **124**, 431 (2001).
 - [49] R. A. Duine and H. T. C. Stoof, *Phys. Rev. A* **65**, 013603 (2001).
 - [50] C. W. Gardiner, J. R. Anglin, and T. I. A. Fudge, *J. Phys. B* **35**, 1555 (2002).
 - [51] C. W. Gardiner and M. J. Davis, *J. Phys. B* **36**, 4731 (2003).
 - [52] N. P. Proukakis and B. Jackson, *J. Phys. B* **41**, 203002 (2008).
 - [53] P. B. Blakie, A. S. Bradley, M. J. Davis, R. J. Ballagh, and C. W. Gardiner, *Adv. Phys.* **57**, 363 (2008).
 - [54] N. G. Berloff and B. V. Svistunov, *Phys. Rev. A* **66**, 013603 (2002).
 - [55] S. E. Hoffmann, J. F. Corney, and P. D. Drummond, *Phys. Rev. A* **78**, 013622 (2008).
 - [56] P. Deuar, *Phys. Rev. Lett.* **103**, 130402 (2009).
 - [57] S. Heller and W. T. Strunz, *J. Phys. B* **42**, 081001 (2009).
 - [58] S. Heller and W. T. Strunz, *ArXiv e-prints* (2010), 1009.3170.
 - [59] M. Brewczyk, M. Gajda, and K. Rzążewski, *J. Phys. B* **40**, R1 (2007).
 - [60] A. Polkovnikov, *Ann. Phys. (N. Y.)* **325**, 1790 (2010).

- [61] M. J. Davis and P. B. Blakie, Phys. Rev. Lett. **96**, 060404 (2006).
- [62] C. N. Weiler, T. W. Neely, D. R. Scherer, A. S. Bradley, M. J. Davis, and B. P. Anderson, Nature **455**, 948 (2008), 0807.3323.
- [63] A. Bezett and P. B. Blakie, Phys. Rev. A **79**, 033611 (2009).
- [64] N. P. Proukakis, J. Schmiedmayer, and H. T. C. Stoof, Phys. Rev. A **73**, 053603 (2006).
- [65] R. A. Duine, B. W. A. Leurs, and H. T. C. Stoof, Phys. Rev. A **69**, 053623 (2004).
- [66] S. P. Cockburn, H. E. Nistazakis, T. P. Horikis, P. G. Kevrekidis, N. P. Proukakis, and D. J. Frantzeskakis, Phys. Rev. Lett. **104**, 174101 (2010).
- [67] B. Damski and W. H. Zurek, Phys. Rev. Lett. **104**, 160404 (2010).
- [68] A. D. Martin and J. Ruostekoski, New J. Phys. **12**, 055018 (2010).
- [69] S. J. Rooney, A. S. Bradley, and P. B. Blakie, Phys. Rev. A **81**, 023630 (2010).
- [70] V. V. Kocharovskiy, V. V. Kocharovskiy, M. Holthaus, C. R. Ooi, A. Svidzinsky, W. Ketterle, and M. O. Scully, Adv. At. Mol. Opt. Phys. **53**, 291 (2006).
- [71] A. A. Svidzinsky and M. O. Scully, Phys. Rev. Lett. **97**, 190402 (2006).
- [72] Z. Idziaszek, L. Zawitkowski, M. Gajda, and K. Rzazewski, Europhys. Lett. **86**, 10002 (2009).
- [73] P. Bienias, K. Pawłowski, M. Gajda, and K. Rzazewski (2010), arXiv:1008.3277.
- [74] M. Sargent III and M. O. Scully, *Theory of Laser Operation* (North-Holland, Amsterdam, 1972), vol. 1 of *Laser Handbook*, chap. A2, pp. 45–114.
- [75] K. V. Kheruntsyan, D. M. Gangardt, P. D. Drummond, and G. V. Shlyapnikov, Phys. Rev. A **71**, 053615 (2005).
- [76] W. Ketterle and N. J. van Druten, Phys. Rev. A **54**, 656 (1996).
- [77] M. Girardeau and R. Arnowitt, Phys. Rev. **113**, 755 (1959).
- [78] C. W. Gardiner, Phys. Rev. A **56**, 1414 (1997).
- [79] M. D. Girardeau, Phys. Rev. A **58**, 775 (1998).
- [80] Y. Castin and R. Dum, Phys. Rev. A **57**, 3008 (1998).
- [81] S. A. Morgan, Journal of Physics B Atomic Molecular Physics **33**, 3847 (2000).
- [82] N. P. Proukakis, S. A. Gardiner, M. J. Davis, N. Nygaard, and M. S. Szymanska, eds., *Non-equilibrium and Finite Temperature Quantum Gases* (World Scientific, Cambridge, to appear in 2011).
- [83] S. Grossmann and M. Holthaus, Phys. Rev. E **54**, 3495 (1996).
- [84] M. Wilkens and C. Weiss, J. mod. Opt. **44**, 1801 (1997).
- [85] M. Bijlsma and H. T. C. Stoof, Phys. Rev. A **55**, 498 (1997).
- [86] K. Burnett, *Proceedings of the Enrico Fermi International School of Physics* (IOS Press, 1999).
- [87] M. Rusch and K. Burnett, Phys. Rev. A **59**, 3851 (1999).
- [88] L. P. Pitaevskii and S. Stringari, Phys. Lett. A **235**, 398 (1997).
- [89] S. Giorgini, Phys. Rev. A **57**, 2949 (1998).
- [90] S. Giorgini, Phys. Rev. A **61**, 063615 (2000).
- [91] P. O. Fedichev and G. V. Shlyapnikov, Phys. Rev. A **58**, 3146 (1998).
- [92] U. Al Khawaja, J. O. Andersen, N. P. Proukakis, and H. T. C. Stoof, Phys. Rev. A **66**, 059902 (2002).
- [93] A. A. Norrie, R. J. Ballagh, and C. W. Gardiner, Phys. Rev. Lett. **94**, 040401 (2005).
- [94] A. A. Norrie, *A Classical Field Treatment of Colliding Bose-Einstein Condensates*, Ph.D. Thesis (University of Otago, Dunedin, 2005).
- [95] B. Berg, L. I. Plimak, A. Polkovnikov, M. K. Olsen, M. Fleischhauer, and W. P. Schleich, Phys. Rev. A **80**, 033624 (2009).
- [96] S. A. Gardiner and S. A. Morgan, Phys. Rev. A **75**, 043621 (2007).
- [97] T. D. Lee, K. Huang, and C. N. Yang, Phys. Rev. **106**, 1135 (1957).
- [98] V. V. Kocharovskiy, V. V. Kocharovskiy, and M. O. Scully, Phys. Rev. A **61**, 053606 (2000).
- [99] S. P. Cockburn and N. P. Proukakis, Las. Phys. **19**, 558 (2009).
- [100] H. T. C. Stoof, Phys. Rev. Lett. **78**, 768 (1997).
- [101] C. W. Gardiner and P. Zoller, Phys. Rev. A **55**, 2902 (1997).
- [102] C. W. Gardiner and P. Zoller, Phys. Rev. A **58**, 536 (1998).
- [103] H. T. C. Stoof, in *Dynamics: Models and Kinetic Methods for Non-equilibrium Many Body Systems*, edited by J. Karkheck (Kluwer, Dordrecht, 2000), vol. 317 of NATO ASI Proceedings, pp. 491–502, arXiv:cond-mat/9812424.
- [104] S. P. Cockburn, *Bose gases in and out of equilibrium within the Stochastic Gross-Pitaevskii equation*, Ph.D. Thesis (Newcastle University, 2010).
- [105] Y. Castin, in *Coherent atomic matter waves*, edited by R. Kaiser, C. Westbrook, and F. David (EDP Sciences and Springer-Verlag, Berlin, 2001), Lecture Notes of Les Houches Summer School, pp. 1–136.
- [106] E. Witkowska, M. Gajda, and K. Rzazewski, Phys. Rev. A **79**, 033631 (2009).
- [107] P. Blair Blakie and M. J. Davis, Journal of Physics B Atomic Molecular Physics **40**, 2043 (2007), arXiv:cond-mat/0508669.
- [108] M. A. Cazalilla and M. Rigol, New J. Phys. **12**, 055006 (2010).
- [109] I. E. Mazets and J. Schmiedmayer, New J. Phys. **12**, 055023 (2010), 0912.4493.
- [110] N. D. Mermin and H. Wagner, Phys. Rev. Lett. **17**, 1133 (1966).
- [111] P. C. Hohenberg, Phys. Rev. **158**, 383 (1967).
- [112] H. T. C. Stoof, D. B. M. Dickerscheid, and K. Gubbels, *Ultracold Quantum Fields*, Theoretical and Mathematical Physics (Springer, 2009).
- [113] O. Penrose and L. Onsager, Phys. Rev. **104**, 576 (1956).
- [114] T. M. Wright, N. P. Proukakis, and M. J. Davis (2010), preprint.
- [115] M. D. Lee, S. A. Morgan, and K. Burnett (2003), arXiv:cond-mat/0305416.
- [116] N. P. Proukakis, Phys. Rev. A **74**, 053617 (2006).
- [117] D. L. Luxat and A. Griffin, Phys. Rev. A **67**, 043603 (2003).
- [118] T. K. Ghosh, Int. J. Mod. Phys. B **20**, 5443 (2006), URL <http://arXiv.org/abs/cond-mat/0402079>.
- [119] L. Mandel and E. Wolf, *Optical coherence and quantum optics* (Cambridge University Press, Cambridge, 1995).
- [120] R. Dodd, C. Clark, M. Edwards, and K. Burnett, Opt. Express **1**, 284 (1997).
- [121] M. Eckart, R. Walser, and W. P. Schleich, New J. Phys. **10**, 045024 (2008).
- [122] R. N. Bisset, M. J. Davis, T. P. Simula, and P. B. Blakie,

- Phys. Rev. A **79**, 033626 (2009).
- [123] C. W. Gardiner and A. S. Bradley, Journal of Physics B Atomic Molecular Physics **34**, 4663 (2001), arXiv:cond-mat/0009371.
 - [124] T. M. Wright, P. B. Blakie, and R. J. Ballagh, Phys. Rev. A **82**, 013621 (2010).
 - [125] P. Meystre and M. Sargent III, *Elements of Quantum Optics* (Springer, Berlin, 1999), 3rd ed.
 - [126] A. L. Shelankov and J. Rammer, Europhys. Lett. **83**, 60002 (2008).
 - [127] R. N. Bisset and P. B. Blakie, Phys. Rev. A **80**, 035602 (2009).
 - [128] L. S. Cederbaum and A. I. Streltsov, Phys. Rev. A **70**, 023610 (2004).
 - [129] R. Grobe, K. Rzazewski, and J. H. Eberly, J. Phys. B **27**, L503 (1994).
 - [130] N. Prokof'ev, O. Ruebenacker, and B. Svistunov, Phys. Rev. Lett. **87**, 270402 (2001).
 - [131] N. Prokof'ev and B. Svistunov, Phys. Rev. A **66**, 043608 (2002).
 - [132] T. Kinoshita, T. Wenger, and D. S. Weiss, Nature (London) **440**, 900 (2006).
 - [133] M. Rigol, Phys. Rev. Lett. **103**, 100403 (2009).
 - [134] K. Rzazewski, J. Mod. Opt. **49**, 2039 (2002).
 - [135] C. Connaughton, C. Josserand, A. Picozzi, Y. Pomeau, and S. Rica, Phys. Rev. Lett. **95**, 263901 (2005).
 - [136] C. C. Marston and G. G. Balint-Kurti, J. Chem. Phys. **91**, 3571 (1989).
 - [137] The global U(1) symmetry holds with the transformation rules $\phi_c \mapsto e^{i\theta} \phi_c$, $u_k \mapsto e^{i\theta} u_k$, $v_k \mapsto e^{-i\theta} v_k$, $n_{th} \mapsto n_{th}$, $m \mapsto e^{2i\theta} m$.